Generic comparison of lumen nucleation and fusion in epithelial organoids with and without hydrostatic pressure

Linjie Lu[†1-4], Kana Fuji[†5], Tristan Guyomar[1-4], Michèle Lieb[1-4], Marie André[1-4], Sakurako Tanida[5-7], Makiko Nonomura[8], Tetsuya Hiraiwa[9,10,5], Yara Alcheikh[12], Siham Yennek[11], Heike Petzold[12], Cecilie Martin-Lemaitre[13], Anne Grapin-Botton*[12,14], Alf Honigmann*[12-14], Masaki Sano*[15,5], Daniel Riveline*[1-4]

[1]Institut de Génétique et de Biologie Moléculaire et Cellulaire, Illkirch, France
[2]Université de Strasbourg, Illkirch, France
[3]Centre National de la Recherche Scientifique, UMR7104, Illkirch, France
[4]Institut National de la Santé et de la Recherche Médicale, U964, Illkirch, France
[5]Universal Biology Institute, Graduate School of Science, The University of Tokyo, Tokyo, Japan
[6]Research Center for Advanced Science and Technology, The University of Tokyo, Tokyo, Japan
[7]Department of Aeronautics and Astronautics, School of Engineering, The University of Tokyo, Tokyo, Japan
[8]Department of Mathematical Information Engineering, College of Industrial Technology, Nihon University, Chiba, Japan
[9]Mechanobiology Institute, Singapore, National University of Singapore, Singapore
[10]Institute of Physics, Academia Sinica, Taipei, Taiwan
[11]The Novo Nordisk Foundation Center for Stem Cell Biology, Copenhagen, Denmark
[12]Max Planck Institute of Molecular Cell Biology and Genetics, Dresden, Germany
[13]Technische Universität Dresden, Biotechnologisches Zentrum, Center for Molecular and Cellular Bioengineering (CMCB), Dresden, Germany
[14]Cluster of Excellence Physics of Life, TU Dresden, 01062 Dresden, Germany
[15]Institute of Natural Sciences, School of Physics and Astronomy, Shanghai Jiao Tong University, Shanghai, China
[†]**Joint first authors**
***Corresponding authors: botton@mpi-cbg.de, alf.honigmann@tu-dresden.de, sano.masaki@sjtu.edu.cn, and riveline@unistra.fr**

Abstract: *Many internal organs in the body harbor a fluid-filled lumen. The mechanisms of lumens initiation and fusion have been reported as dependent on organ-type during organogenesis. In contrast, the physics of lumen suggests that force balance between luminal pressure and cell mechanics could lead to conserved rules which may unify their self-organisation. However, this hypothesis lacks experimental evidence. Here we compare lumen dynamics for three different systems (MDCK cysts, pancreatic spheres, and epiblast cysts) by using quantitative cell biology, microfabrication and theory. We report that initial cell number determines the maximum number of lumens but does not impact the steady state which is a final single lumen. In addition, lumen numbers exhibit two phases over time, a nucleation phase followed by a fusion phase. In the nucleation phase, lumens form between two cells in pancreatic and MDCK cysts whereas they form at the rosette stage between ten cells in epiblasts. In the second phase, lumens fuse by an increase in lumen volume for pancreatic spheres and MDCK cysts, whereas cell convergent directional motion leads to lumens fusion in epiblasts. We show that these phenomena are associated to the luminal hydrostatic pressure. We support these results with theoretical arguments and numerical simulations. We finally use MDCK cysts to manipulate cell adhesion and lumen volume and we successfully* reproduce the fusion dynamics of pancreatic spheres and epiblasts. Our results reveal self-organisation rules of lumens across systems with relevance for morphogenesis during development and for the design of synthetic *organs.*

Introduction.

Organogenesis relies on individual cells that proliferate and interact to self-organise. An interplay between the physical properties of cells, their tissue organisation, gene expression, and molecular control sets the complex rules for morphogenesis[1,2]. The cells in different organs use common means of controlling cell division, cell volume and shape, cell rearrangement and migration to enable different shapes to emerge[3]. Basic physical parameters of cells, such as pressure differences or surface tension, are crucial to the process. Understanding the physics of organogenesis requires clarifying these generic rules applicable to different cell types.

We took a generic approach to study the dynamics of a central structure in organs, *i.e.,* the lumen. Although lumen formation occurs in different epithelial organ models, several mechanisms of lumen formation are conserved across multiple systems such as hollowing after cell division[4–8] or by apoptosis leading to cavitation[7–9]. In addition, theory for the physics of lumen was proposed[10,11] and some physical mechanisms for its dynamics were reported experimentally[12,13]. A systematic comparison between cellular systems is lacking so far.

Here, we probed self-organisation of lumens on *in vitro* models. We use epithelial organoids as paradigms for lumen dynamics with physiological relevance[14–19]. We report a universal trend in various model systems, *i.e.* an increase in the number of lumens as a function of time followed by a decrease due to fusion until they all reach a single lumen. We also show that epithelial-derived lumens nucleate either after cell division or upon cell contact whereas epiblasts form lumens when they reach a rosette stage of 10 cells. By contrast, fusion of lumens is dominated by increase in pressure for pancreatic and MDCK spheres, whereas epiblast lumens fuse by cell motion. We show that epiblast lumens have negligible hydrostatic pressure in contrast to MDCK and pancreatic spheres. These rules are substantiated with a numerical simulation reproducing cell dynamics and lumen appearance using a phase field approach and by theoretical arguments. To further test these mechanisms, we used MDCK cysts to manipulate adhesion and lumen volume and we successfully reproduce the fusion dynamics of pancreatic spheres and epiblasts.

Results.

Distinct phases of lumen dynamics

To track the growth and morphology of organoids (Fig. 1), we designed a microwell-containing device optimized for cell imaging and cyst tracking by using soft lithography[20] (Fig. 1a and Materials and Methods). Single devices contained microwells of different diameters adjusted to the measured mean cell dimension of each cellular system and a constant height equal to the cell height (Ext. Fig. 1). This allowed us to follow different initial cell numbers over time within the same experiment, *i.e.,* 1, 2, 3, 4, 8, 16 cells (Fig. 1c). We used an MDCK cell line which expressed markers for cell-cell junctions and for lumens (see Materials and Methods) and this allowed us to track in three dimensions the number of lumens as a function of time in three dimensions (Fig. 1b-e). We observed two phases, Phase I with an increase in the number of lumens during the first 24 hours followed by Phase II with a decrease over time eventually reaching a single lumen. This suggests that cells formed new lumens over time and that these lumens underwent fusion irrespectively of their initial number. During Phase II, these lumens

could also undergo fusion irrespectively of their initial number and cyst shape (Fig. 1f,g). In addition, larger initial cell numbers correlated to larger number of lumens, ranging from a peak of 1 lumen for 1 initial cell at 24 hours to 6 lumens on average for 16 initial cells. They reached single lumen within 24 hours (1 day) for 1 initial cell and 192 hours (8 days) for 16 initial cells.

We further explored whether this biphasic behavior was conserved in other systems. We plated pancreatic cells freshly isolated from fetal mouse pancreases at 13.5 days of development in the micro-cavities with adjusted dimensions and we tracked the evolution of lumen number over time (Fig. 2a and Fig. 2b). We quantified these dynamics (Fig. 2b) and we found a biphasic trend similar to the MDCK system (Fig. 1e). However, the distribution ranged from a peak of 1 lumen for 1 initial cell at 16 hours to 5 lumens on average for 16 initial cells. Lumens fused into a single lumen within 24 hours and 48 hours respectively. The same experiment with epiblasts led to similar conclusions (Fig. 2c and Fig. 2d): the lumen numbers increased and then decreased reaching single lumens, ranging from an average peak of 1 lumen to 4 lumens for initial cell numbers of 1 cell and 16 cells respectively. Lumen fusion into a single lumen happened within 2 days and 3 days respectively. Altogether all systems exhibited the same qualitative behavior, increase in lumen number with increasing initial cell numbers, and an increase of lumens number followed by fusion leading to single lumens.

The three systems exhibited similar phases but with a different timing. We hypothesized that this may be due to different cell cycle lengths of the different cell types. We thus plotted the number of lumens per cell cycle as a function of initial cell number for each system (Fig. 3a). Remarkably, the curves were similar for MDCK cysts and pancreatic spheres with an increase of 0.2 lumen per cell cycle per initial cell number. In contrast, the slope was 5 times smaller for epiblasts, suggesting differences in the nucleation mechanisms. Following the dynamics of MDCK cells we could see that lumens formed by two mechanisms (Fig. 3b and Movie 1). As described previously, cells nucleated a lumen in the middle of the cell-cell contact after cell division[6,21] (see time 1:40 top Fig. 3b and Ext. Fig. 3a). In addition, we found that two cells formed a lumen when they adhered to each other (see time 2:00 bottom Fig. 3b and Movie 2). The time needed for lumen appearance was similar between both processes (Fig. 3c). Both mechanisms were also observed in pancreatic cells (Fig. 3d, Movie 3 and Movie 4) with the same 2 hours timescale typically required to nucleate a lumen (Fig. 3e). It is worth noting that the low number of lumens per cell cycle per initial cell number suggests that lumens are nucleated during this Phase I but also undergo fusion with other lumens. The mechanism of nucleation was in sharp contrast with the appearance of lumens in the epiblasts (Fig. 3f and Fig. 3g): the lumen nucleated only when a critical number of about 10 cells formed a rosette (see time 48h in Fig. 3f and Fig. 3g and Ext. Fig. 3b and c). This may explain the distinct dynamics in Phase I.

Hydrostatic pressure driving lumen fusion in epithelial models

The decrease in lumen number seen over time in Phase II suggested that lumen disappeared by fusing together (Fig. 4a). Live imaging enabled us to observe and quantify lumen fusion. We plotted the lumen fusion per cell cycle as a function of initial cell number (Fig. 4a). Unlike for Phase I, the three systems exhibited different fusion rates. The fusion was the fastest in pancreatic spheres with a reduction of lumen at a rate of 0.1 per cell cycle per initial cell number, followed by the epiblasts with a reduction of 0.08 per cycle per initial cell number. In contrast the decrease was about 3-fold slower smaller for MDCK lumens fusions than for the other organoids. To further compare the systems, we followed the dynamics of fusion of cysts for initial conditions of 8 cells until cysts reached similar dimensions and cell numbers

(Fig. 4b). MDCK cysts exhibited a striking dynamic: the nearest neighbouring lumens coming to contact fused by breaking the cellular junctions separating them over 60 hours (Fig. 4b and Movie 5). We quantified these dynamics by plotting the lumen index (LI) per lumen; LI quantifies the ratio between the luminal area and outer cyst area to capture the respective increase in lumen volume (Fig. 4c, see Materials and Methods). The LI of one lumen increased whereas the LI of the neighbouring lumens decreased in the period preceding the fusion. This sequence of events was similar for pancreatic sphere fusion but with faster kinetics (Fig. 4b and Movie 6) as evidenced in the LI quantification (Fig. 4d). In contrast, when we tracked the fusion of epiblasts lumens (Fig. 4b and Movie 7) we did not see a significant increase in the LI as illustrated by a constant LI prior to fusion (Fig. 4e). The large LI (approximately 1) for pancreatic spheres may suggest that the luminal pressure is larger than the MDCK sphere which presents a lumen index of 0.3 which is again 3-fold higher than the epiblast LI (see Ext. Fig. 4c). This indicates that increase in luminal pressure is large and important in pancreatic and in MDCK spheres. If hydrostatic pressure is a driver of fusion, we reasoned that it must rip apart the adhesion between cells separating two lumens. To gain insight into adherens junctions, we quantified the levels of E-cadherins levels at junctions (see Fig. 5ab and Ext. Fig. 5c). The mean concentration of E-cadherin was much larger for MDCK spheres compared to the other systems, which suggests that adhesion force may counteract lumen fusion via luminal pressure in this system. This difference in adhesion was further supported by inflation experiments where the cell layer was more easily disrupted in epiblast than in MDCK spheres (Ext.Fig. 5d). This feature can explain the lower slope for the lumen fusion for MDCK cysts compared to pancreatic spheres which may be dominated by large luminal pressure and low adhesion (Fig. 4a).

To test this central role for luminal hydrostatic pressure, we performed drainage experiments designed in our former study[22](see Materials and Methods, Ext. Fig.6 and Fig. 5d-g). By cutting locally the cell layer with a laser, we could evaluate the luminal hydrostatic pressure associated to each cyst. Our results show that MDCK cysts have a hydrostatic pressure of 65Pa, larger than pancreatic spheres[23], in contrast to epiblast which have a hydrostatic pressure close to 0Pa. We also tested that the mechanical properties of monolayers were similar (Ext. Fig. 7), supporting the notion that luminal pressure was the driving force for nucleation and fusion of lumens.

Motion-directed lumen fusion in epiblasts

Since the slope of lumen fusion was much lower for MDCK cysts than pancreatic spheres and epiblasts, we sought for an alternative mechanism driving lumen fusion. The lumen index value of epiblasts suggests that luminal pressure does not play a key role in the fusion. In particular the neighbouring rosettes compacted into a sphere in epiblasts (Fig. 4b) and this was associated to the transformation of the outer layer of the cyst from an elongated shape to a sphere (Fig. 4i) in contrast to MDCK fusion case where the cyst remained spherical (Fig. 4f). We then measured the distance gained along the long axis of the cyst by cells: they corresponded to the distance needed for the lumens to fuse (Fig. 4j,k, see Materials and Methods). This is in sharp contrast with MDCK cysts (Fig. 4g,h). These experiments suggest that lumens fusion in epiblasts are driven by cells convergent directional motion associated with changes in cyst shape, whereas lumens fusions are mainly mediated by luminal pressure for MDCK cysts and pancreatic spheres.

Toward quantitative generic rules for lumen dynamics

We turned to numerical simulations to reveal the rules in cell proliferation, cell adhesion, lumen formation and luminal pressure, which could reproduce the main results across systems. These *in silico* experiments enabled us to test the hypotheses derived from our observations. In this context, we selected the phase field model which captures the complex dynamics of cells and lumens once a proper free energy is set[24–26]. We assumed that cells grow and divide at threshold time and volume and form a lumen (Fig. 5a) and we modulate the increase in lumen volume and control cell-cell adhesion (see Suppl. Note). In silico experiments evolve spontaneously by setting the initial conditions as in the real experiments. We illustrate typical evolutions of the numerical cysts with 8 cells as initial cell number with the knowledge of the respective proliferation time of our systems, the same doubling time for MDCK and pancreatic spheres and stronger adhesion force for MDCK cells (Fig.5). We obtained phenotypes similar to MDCK cysts (Fig. 6b blue, see also Movie 9); for larger luminal pressure with the same proliferation time (green), fusion looked similar to pancreatic spheres (Movie 10). Quantifications of lumen index in the numerical cysts for each case reproduced also the quantifications of experimental lumen index (compare Fig. 6d with Fig. 4c). Finally, to further validate the relevance of our simulations to experimental data, we quantified the dynamics *in silico* of the systems from initial stages by counting the number of lumens as a function of time. Strikingly we could reproduce the biphasic behaviour for all systems (Fig. 6c). These simulations support the importance of the interplay between cell proliferation, cell adhesion and luminal growth in setting quantitatively lumen dynamics across systems.

Based on our result of zero luminal pressure for epiblasts, we turned to alternative mechanisms. We analytically evaluated the number of cells needed to nucleate a lumen in the absence of hydrostatic pressure by assuming a similar free energy with the phase field model (Fig. 6e-h and Supplementary note). Our results show that 10 cells are needed to nucleate a lumen (see Fig. 6e,f) in good agreement with our results for epiblasts whereas 2 cells are sufficient for a cyst with luminal pressure (Fig.6g and 6h). This difference substantiates the differences between MDCK/pancreatic spheres on the one hand and epiblasts on the other hand.

Testing the model in MDCK cysts and epiblasts

Our modeling and experimental observations suggested that lumen growth, adhesion between cells and cellular properties governed the differences between the three systems. We further tested this experimentally using the MDCK system as a reference and perturbing these parameters. To evaluate the role of lumen growth in fusion, we prepared MDCK cysts with two lumens and we designed an inflation experiment using a micro-pipette to inject fluid[22] (Fig. 7a and Ext. Fig. 8). To show the fusion, we used dextran in the pipette. We could induce the fusion within minutes. This suggests that an increase in lumen growth rate can drive fusion of MDCK lumen faster than it normally takes, along the result of a faster response promoted by an increase of lumen volume in pancreatic spheres. In contrast, epiblast could not sustain this volume change upon injection, leading the whole structure to collapse instead of triggering fusion (Ext. Fig 9). The same enhanced fusion was obtained by an osmotic shock (Fig. 7b and 7c and Materials and Methods). In addition, the apparent role of cell-cell adhesion for MDCK cysts was further tested by simultaneously decreasing cadherin-mediated adhesion by chelating calcium with EDTA and using an anti E-cadherin blocking antibody[27,28] (Fig. 7d). We observed that lumen number is significantly decreased, suggesting that lumen fusion was facilitated (Fig. 7d, e). This suggests that adhesion between cells is an impediment to fusion in MDCK cysts. In addition, we tested the behaviour of E-cadherin KO MDCK cell line for 8 cells and 16 cells initial conditions: the biphasic behaviour was reproduced but this E-cadherin cell line presented a faster fusion (see Fig. 7f,g,h). This further confirms

that adhesion between cells can prevent fusion. Finally, to test the impact of cellular properties on lumen formation, we used a MDCK cell line in which the tight junction proteins ZO1 and ZO2 were knocked-out[22,29]. This cell line was shown to have smaller LI due to increased apical contractility[22] and resembled the epiblast case with smaller lumen and elongated cells (see Ext. Fig. 10a). We initiated the MDCK ZO-1/2 KO2 KO cysts with 1 to 16 cells and we repeated the observation of the number of lumens as a function of time and initial cell numbers (Fig. 11a, b). The results show that fusion was facilitated in the ZO-1/2 KO cyst. Several features of this ZO-1/2 KO MDCK cyst corresponded with epiblasts cysts, such as low LI and similar mechanical response to inflation (Ext.Fig. 10b), as well as facilitated fusion as a function of cell number. This suggests that tight junction deletion contributes to faster fusion. These experiments of MDCK cysts transformations with mechanical or biological perturbations support the notion that lumen fusion generically results from this interplay between luminal pressure and mechanical cell interactions.

Finally, to show that activity was required for the fusion in the case of epiblasts, we recorded the fusion of epiblasts in the presence of the myosin inhibitor, blebbistatin (Fig. 8a). Fusion was prevented, which shows that active forces are needed to promote fusion. This was also obtained when adhesion was reduced in MDCK ZO-1/2 KO (Ext. Fig. 10c). To further substantiate these fusion mechanisms with no pressure, we prepared numerical epiblasts similar to the experimental system with two lumens and small luminal pressure (Movie 11) with an elongated configuration similar to the experimental case (compare Fig. 4b). Based on experimental measurements in this configuration (Fig. 4i-k), we imposed radial cell motion by adding active forces (Fig. 8b) and we successfully recapitulated the fusion (Fig. 8c) as well as cell motion within the cyst (Fig. 8d,e) and axis ratio of the cyst (Fig. 8f).

Discussion.

We have shown that the number of lumens depends on the initial cell number and their evolution exhibits similar biphasic behaviours for MDCK, pancreatic spheres and epiblasts (Fig. 7). The nucleation phase is dictated mainly by appearance of new lumens whereas the second phase is dominated by fusion to reach a single lumen for all systems. Nucleation mechanisms are shared between MDCK cells and pancreatic spheres both when cells divide and when two cells adhere to each other, whereas epiblasts need about 10 cells to nucleate a lumen. MDCK and pancreatic spheres fusions are predominantly driven by an increase in lumen index and high pressure, whereas fusion is determined by active cell motion in epiblasts with low lumen index and negligible pressure. Our experimental perturbations of MDCK fusions suggest that luminal pressure in competition with cell-cell adhesion controls fusion. In pancreatic spheres the lumen index is larger than the MDCK cysts and fusion is likely driven by luminal ion pumping, whereas epiblasts fusions are dominated by cells motion.

The mechanism of lumen nucleation after cell division has been reported for MDCK cells[6,30,31]. It is consistent with the nucleation mechanism we report for MDCK and we report it for pancreatic spheres. In addition, we also add the lumen nucleation associated to contact between cells as well, which supports the notion that several mechanisms of lumen nucleation could co-exist with similar timing. It is worth noting that lumen nucleation was reported in an assay between a cadherin coated surface and a single cell[32] suggesting that adherens junctions formation between cells *per se* could trigger lumen formation. Finally, we report that the larger number of cells is needed to nucleate a lumen in epiblasts

and it is consistent with Shahbazi *et al*[33,34]. Despite these multiple mechanisms for lumen nucleation, we report and explain in a unified way the mechanisms for the nucleation, i.e. Phase I, across systems.

We distinguish fusion between lumens triggered by ion-pumping mechanisms leading to an effective increase in hydrostatic pressure of the lumen in competition with cell-cell adhesion and fusion between lumens triggered by cell re-organisation. This difference can be understood by a simple force balance argument: when the lumen index is large, the hydrostatic pressure of the lumen pushes the cell apical side and the cell monolayer thereby competing with cell-cell contacts; in contrast, when lumen index is low, the hydrostatic pressure of the lumen is low and interactions between cells essentially determine the potential fusion between lumens. Lumen fusion by increased osmotic pressure was reported in various situations *in vitro* and *in vivo*[12,35,36] along our observations and this illustrates that common rules of self-organisation across systems could determine the morphogenesis of organs in 3D.

It is interesting to understand why epiblasts show very low hydrostatic pressure. We note that MDCK cysts and pancreatic spheres are sealed in the sense that Dextran cannot enter the luminal space[22,23]. This is in sharp contrast with epiblasts[34,37]. We propose that this difference is associated with low luminal pressure. In addition, we conjecture that this property is associated to tight junction maturation, *i.e.* tight junctions are fully matured in MDCK cysts whereas they do not reach this state in epiblasts. This proposition is consistent with the similar lumen dynamics exhibited by epiblasts and by ZO-1/2 KO MDCK cell lines. Future experiments will be needed to identify the molecular mechanisms associated to tight junction maturation.

We propose that these nucleation and fusion mechanisms could be tested on other organoid systems. The timing of cell proliferation compared to lumen fusion dynamics could be tuned to optimize the target size of the organ with the relevant cell number and the number and size of lumens. Systems may select fast pumping like the pancreas to allow multiple lumens to fuse rapidly with potential change in luminal pressure to form a single duct[38]. By contrast, systems that would need to keep compartments such as the thyroid gland may have developed larger adhesion properties to prevent fusion and allow each zone to keep potential differences in composition[39].

In considering functional differences between cells connected to lumen dynamics, it is interesting to note that cells change their states in the case of epiblasts[40]. From stem cells, they exit from pluripotency and follow paths of differentiation leading to the right localization in the final organs. We propose that this orchestration of proliferation with lumens nucleation and fusion could also be optimized to generate organs with the relevant shape and cell numbers but also with the correct cell-state distributions. Future experiments coupling our approach with spatial transcriptomics will allow to test this hypothesis.

Our results could shed light on the synthesis of artificial organs. Indeed, it was reported that cell printing was a promising method to generate organs[41,42]. Our results show that the cell number at plating, their growth rates, and their fusions, contribute to the dynamics of the organs formation. This initial condition correlates with morphology and functions of organ. As a result, a due care to the force balance would need to be evaluated in the synthesis of organs and our framework with its numerical simulations could serve as a solid basis to predict the future shape of the targeted organs.

Acknowledgements.

We thank the Riveline group for help and discussions and Erwan Grandgirard and the Imaging Platform of IGBMC, Patrick Reilly for assistance in editing. We also thank Byung Ho Lee and Allison Lewis for experimental, conceptual and image analysis advice and discussions. We thank Benoît Ladoux for providing the MDCKII E- cadherin KO cell line. L.L. and T.G. are supported by HFSP and by the University of Strasbourg and by la Fondation pour la Recherche Médicale. D.R. acknowledges the Interdisciplinary Thematic Institute IMCBio, part of the ITI 2021-2028 program of the University of Strasbourg, CNRS and Inserm, which was supported by IdEx Unistra (ANR-10-IDEX-0002), and by SFRI-STRAT'US project (ANR 20-SFRI-0012) and EUR IMCBio (ANR-17-EURE-0023) under the framework of the French Investments for the Future Program. A.G.B, A.H., M.S. and DR acknowledge the Research Grant from Human Frontier Science Program (Ref.-No: RGP0050/2018).

Materials and Methods.

Cell sources and expansion

We used 3 cellular systems, MDCK II cell lines, mouse embryonic cells (mES cells)[43], and pancreatic spheres[44]. Other mutant cell lines were used for MDCK: MDCK II E-cadherin-GFP/Podocalyxin-mScarlett/Halo-CAAX[45], MDCK II ZO1/2-KO[22] and MDCK II E-cadherin KO[46].

The MDCK II cell lines were cultured in MEM (Gibco 410900028) with 5 % Fetal Bovine Serum (Sigma, USA), 1mM Sodium Pyruvate (Gibco 11360-070) and 1x NEAA (Gibco 11140050). MDCKII cells were resuspended every 2 to 3 days with trypsin-EDTA after they reached 70-95% confluency. A seeding density of about $3*10^5$ cells per 75 cm^2 was used for sub-culture. R1 ES-cell line was used for the culture of epiblast (quote 25). Mouse embryonic stem cells were expanded with 1:1 DMEM/F12 (ThermoFischer 31331028) and neurobasal medium (Gibco 21103049) supplemented with 1x N2 (Gibco 17502048), 1x B27 (Gibco 12587010) and 1x NEAA (Gibco 11140050), 55µM 2-Mercaptoethanol (Gibco 21985023), 3µM CHIR 99021 (Sigma SML 1046-5mg) and 2x LIF produced at IGBMC-Strasbourg in non-adhesive flasks[43]. Cells were sub-cultured every 4 days until the size of spheres reached a diameter of 80µm. Pancreatic spheres were prepared from the dissection of E13.5 embryos (mouse CD1 from Charles River Laboratory) using the protocol reported in Greggio et al[44] and used without passaging.

Cells diameter measurement.

For the three systems, single cells were plated after trypsinisation and labeled using 10nM SiR-actin (TEBU-BIO, 251SC001). The middle planes of spherical cells were imaged. The associated surfaces were measured with Fiji and the distributions of cells diameters were plotted (see Ext. Fig. 1). Cavities

diameters were designed accordingly by taking the mean value of each distribution to control the initial cell numbers (Ext. Fig. 1c). All cavities had a cell height from 10µm to 17µm to keep the height similar to one cell diameter.

Microfabrication and cavity map.

We designed the samples with a map of patterns for cavities in order to: (i) track the evolution of the same cysts up to a week, (ii) test a large number of cysts with the same initial cell number and (iii) test the effects of different initial cell numbers for the same biological repeat (see Fig. 1a). The same strategy was adapted for each system by designing the cavity map accordingly.

Cavities were prepared using soft lithography as described in Bhat et al[20]. Briefly, we designed a mask with
AutoCad to obtain a large number of motifs and different diameters. The motifs were selected to contain many initial cells number conditions. We used the following calculation of the motif's diameter, rescaled with the mean cell diameter: S(surface of cavities)= number of initial cells*surface of cells. These designs were printed on photomask and then we transfer these patterns on SU-8 silicon wafer with soft lithography. Next the design was replicated on a PDMS mold. Finally, these designs were transferred to cover-glass which allows us to achieve higher resolution images.

Cell seeding in microfabricated cavities for the control of initial cell number.

To generate cysts and organoids in micro-fabricated cavities, we seeded cells in micro-cavities with the following steps based on our former protocol[20,47]. Briefly, (i) the microfabricated-cavities on coverslips were activated with O_2 plasma (Diener); (ii) substrates were incubated with 5µg/ml laminin (Sigma 11243217001) for 1 hour at room temperature followed by washing steps; (iii) cells in suspension were centrifuged 3 times at 1000 rpm for 3 minutes on the samples to direct cells inside micro-cavities; (iv) the coverslips were then rinsed gently to get rid of the excess of cells between cavities; (v) 15 µl Matrigel (Corning, 356231) was added on top of the sample. After solidification of the Matrigel, the relevant media were added depending on the cyst types. For pancreas spheres, single cells were dissociated from the E13.5 pancreases and immediately seeded in the micro-well without centrifugation.

System-specific media were added to obtain pancreatic spheres or epiblasts. Pancreatic sphere was formed by using DMEM/F12 (ThermoFischer 31331028) with B27 (Gibco 17504-044), recombinant Human FGF2 (R&D 233-FB-025), Y-27632 (Sigma Aldrich ab120129) and Penicillin-Streptomycin (Gibco 15070-063)[44]. Epiblasts were differentiated by using 1:1 ratio of DMEM/F12 (ThermoFischer 31331028) and neurobasal medium (Gibco 21103049) containing 0.5x N2 (Gibco 17502048), 1x B27 with vitamin A (Gibco 12587010), 1x NEAA (Gibco17504044), 0.1mM 2-Mercaptoethanol (Gibco 21985023), 0.15mM Sodium Pyruvate and 0.2mM LGlutamaine (Life Technology GmbH 11360039).

Immunostaining.

For immunostaining, we followed standard protocols Greggio, C. et al[45,48]. Briefly, samples were washed with PBS and fixed with 4% paraformaldehyde (Electron Microscopy Sciences 15710) diluted in PBS for 15 minutes. Cells were permeabilized with 0.5% Triton-X-100 for 15 minutes and then a blocking solution made of 1% Normal Goat Serum in PBS 1X was added overnight. Primary antibodies were

added directly to the blocking solution for two days at 4°C. Following 3 successive washing steps with PBS, the samples were stained with the relevant secondary antibodies for 2 hours at room temperature. We used the following primary antibodies: Anti-E-cadherin (Abcam, Ab11512 and Ab53033), Mouse monoclonal Anti-Podocalyxin (BIO-TECHNE SAS, MAB1556-SP), Alexa Fluor Phalloidin 488 (ThermoFisher, A12379) for F-actin and DAPI (Sigma MBD0015) for the nucleus. Samples were washed three times in PBS and mounted on a home-made sample holder system for imaging and conservation.

Microscopy.

In order to track the number of lumens in MDCK cysts, MDCK cells expressing Ecad – Podxl were used to visualize adherens junctions and apical side, respectively. After cell seeding, images were taken at an interval of 24 hours using Leica DMI8 with an Evolve 512 camera coupled to a spinning disk microscope (CSU W1) with a 25x water objective (NA = 0.9) and 63x glycerol objective (NA = 1.2) using the software Metamorph for image acquisition. Positions were chosen based on initial cell numbers and the same MDCKII cysts were acquired in 3D every 24h. This was possible with the cavity map reported above. For pancreatic spheres and epiblasts, initial conditions were controlled with the same method and samples were fixed and stained with the relevant antibodies before 3D acquisition with the same microscopy setup.

To record the lumen formation in MDCK, MDCK cysts were imaged at a time interval of 5 min for more than 24 hours in a setup regulated for 5% CO_2 and 37°C temperature. We used MDCK cells stably expressing E-cadherin-GFP and podocalyxin as readouts for cells junction and lumen. To record the lumen nucleation in pancreatic spheres, we imaged them live after cells seeding with phase contrast microscopy (Fig. 3d). For the characterisation of lumen nucleation in epiblasts, we fixed samples with every 8 hours after cells seeding and we stained for E-cadherin and podocalyxin prior imaging (Fig. 3f).

For lumen fusion events in MDCK cysts, we used a 63x glycerol objective (N.A.= 1.2). Different organoids were selected as starting positions and imaged every 30 min for up to 3 days. Z-stacks (60 µm range, 1 µm step) were acquired. For lumen fusion in epiblasts, epiblasts were imaged from day 2 with SiR-actin (TEBU-BIO, 251SC001) after 1 hour incubation before the experiment. Then SiR-actin mix were incubated with media leading to a final concentration of SiR-actin and Verapamil. The concentrations were larger for MDCK cysts for optimal visualisation. Lumen interaction events were recorded with a Leica CSU-W1 spinning disk (63× objective) for more than 10 hours at an interval time of 30 min.

Perturbation experiments.

For the inflation experiment[22] (Fig. 7a), MDCK cysts were used after 5 days of culture. We first removed gently Matrigel from the top of micro-wells with a needle. The lumen was inflated by flowing media containing fluorescent dextran (Fisher Scientific SAS D22914) in the relevant media with a micro-pipette and images were taken using Leica spinning disk equipped with micromanipulators. For osmotic shock, we incubated the sample with 300 mM D-mannitol solution (Sigma M9546).To investigate the role of adhesion in lumen fusion, we used 5 mM EDTA and E-cadherin 10 µg/ml antibody [27,28] (Fig. 7b). Snapshots of MDCK cells were taken right before addition of EDTA/E-cadherin antibody and then the cysts were acquired in 3D for 60 minutes to record the fusion events. To interfer with cell motion during

fusion in epiblasts, we used the myosin inhibitor blebbistatin (Sigma B0560) at 10 µM with a DMSO sample for control. For the hydrostatic pressure measurement and lumen drainage, we used our established method. Hydrostatic pressure was calculated based on the Hagen-Poiseuille model. Channel dimensions were confirmed through combined fluorescence and transmission light imaging, ensuring accurate assessment of channel size and pressure parameters[22,23]. Surface tension measurements were based on established methods[49].

Imaging and data analysis.

To extract the shapes and measure the volumes and surfaces of lumens and organoids, we used LimeSeg Fiji Plugin and Skeleton Seg. The segmented 3D structures were saved and visualized. Analysis and quantification were performed with Paraviewer[50].

The number of lumens were rescaled with respect to the cell cycle (Fig. 3a and Fig. 4a) by dividing the number of lumens by the duration of each cell cycle. We took 18h for MDCK, 18h for pancreatic spheres, and 9h for epiblasts. We checked that doubling times were consistent with the number of cells counted in each system. In addition, we define lumen as a fluid-filled cavity between cells within the optical resolution together with accumulation of apical marker such as podocalyxin and F-actin. Lumen index is defined as the ratio between the area of lumen and the area of the outer shell of the cyst. They were measured for each system. The numerical lumen index was measured by taking 2D lumen surface over cyst surface. To compare the fusion process between MDCK cyst and epiblast, we ellipse fitted the outer contour of cysts to extract the long and short axis. Then, we plotted the major axis over the minor axis as a function of time (Figure 4f,i). To characterize the associated cell motion during fusion, we plotted cell trajectories by using tracking their centers (Figure 4h,k).

Data were plotted using a written Python code and GraphPad Prism. Statistical tests were performed using non-parametric Mann-Whitney test (two-tailed) to evaluate the significance between lumen formation after cell division and when cells met (Figure 3c,e), lumen occupancy (Fig. 5b), intensity of E-cadherin (Fig 5c), and the difference of number of lumens between WT MDCK cyst and ZO-KO cyst (Figure 6h). The differences of number of lumens before and after EDTA+ anti-E-cadherin treatment were assessed for statistical significance by using Wilcoxon matched-pairs signed rank test (Figure 7e). Differences between groups for the pipette inflation experiment were analysed for statistical significance by ANOVA. Statistical significance was indicated using the following symbols: ns p-value >0.05, * $p < 0.05$, ** $p < 0.01$ and *** $p < 0.001$.

The number of experimental repeats and number of cyst or organoids are indicated in the Figure captions.

Theoretical model and numerical simulations.

The cyst was theoretically modeled based on the multi-cellular phase field model with lumen[25] but additionally incorporating the extracellular matrix around the cyst. To carefully control the surface

tension of each entity (each cell, lumen, ECM), we applied the resharpening method proposed in Refs. [51,52], which enabled us to eliminate the surface tension artificially generated due to the construction principle of the phase field model. The details of this theoretical model are given in Supplementary Note Theory.

Materials, Data and Code availability.

All materials will be available upon reasonable request.

The Data are available upon request and the software Code used for the simulation is available in the Github, https://github.com/kana-fuji/MCPFM_for_Lumen_Fusion.git

----

Movies Captions.

Movie 1 - Lumen nucleation after cell division for MDCK cyst. MDCK cells expressing E-cadherin in green and Podocalyxin. Time in hh:mm:ss.

Movie 2 - Lumen nucleation after cells meet for MDCK cyst. MDCK cells expressing E-cadherin in green and Podocalyxin. Time in hh:mm:ss.

Movie 3 - Lumen nucleation after cell division for pancreatic sphere. Time in hh:mm.

Movie 4 - Lumen nucleation after cells meet for pancreatic sphere. Time in hh:mm.

Movie 5 - Lumen increase in volume leads to lumen fusion for MDCK cyst. MDCK cells expressing E-cadherin in green and Podocalyxin in red with 8 cells as initial conditions. Time in hh:mm.

Movie 6 - Lumen increase in volume leads to lumen fusion for pancreatic spheres. Pancreatic spheres were imaged with 8 cells as initial condition. Time in hh:mm.

Movie 7 - Centripetal motion with low lumen occupancy leads to lumen fusion in epiblast. Time in hh:mm.

Movie 8 - Simulation movie of typical numerical evolution of cysts.

Movie 9 - Simulation movie of lumen interaction and fusion for 8 cells condition – with a dynamic similar to MDCK cyst.

Movie 10 - Simulation movie of lumen interaction and fusion for 8 cells – with a dynamic similar to pancreatic sphere.

Movie 11 - Simulation movie of lumen fusion for 8 cells condition – with a dynamic similar to epiblast.

Figures Captions

Figure 1 - Lumen nucleation and fusion in MDCK spheroids with controlled initial cell numbers. a. Mask for the design of the cavity map. Cavities of different diameters were arrayed and designed to accommodate different initial cell numbers. b. Schematic representation of lumenogenesis. Dissociated plated cells adhere to each other and then lumens (surrounded by red line) are nucleated and eventually fuse. c. Typical dynamics of MDCK cysts forming from controlled initial cell numbers (E-cadherin in green, Podocalyxin in red). Initial cell numbers are shown at time 0 in cavities (scale bar) and the shapes of the same spheroids are captured every day. The yellow line outlines the zone of MDCK cysts which reached the single lumen stage. Scale bar 10µm (N=3, n≥ 10). d. 3D visualization of four lumens and spheroids corresponding to c and indicated as 1,2,3,4. left: 3D viewer of spheroids with E-cadherin in green and Podocalyxin in red. Right: 3d viewer of lumen by Imaris. e. Quantification of the number of lumens in MDCK spheroids as a function of time for different initial cell number: 1,2,3, 4, 8, 16 cells. Each point represents an individual cyst, while the dark line corresponds to the mean value, and the shaded region indicates the standard deviation. The number of lumens increases over time and with initial cell number. All cysts end up close to single lumens. (f,g) External control of MDCK cyst growth using micro-well confinement. Comparison of lumen nucleation in circular and rectangular micro-wells shapes varying initial cell numbers. Podocalyxin is labeled in red and E-cadherin is labeled in green. (g) Representative images show cyst morphology at Day 0 (left) and Day 4 (right). Scale bars: 20µm in f and in g.

Figure 2 - Lumen nucleation and fusion in pancreatic and in epiblast spheres. a. Typical evolution of pancreatic spheres shapes as a function of initial cell number and time (F-actin in green, nucleus in Magenta) (N=3, n>20). Scale bars 10µm at time 0 and at time 96 h with 3D zooms on outlined pancreatic spheres. b. Quantification of the number of lumens in pancreatic spheres as a function of time for different initial cell numbers: 1,2, 4, 8, 16 cells. c. Typical evolution of epiblasts as a function of initial cell number and time (E-cadherin in green, Podocalyxin in red) (N=3, n>20). Scale bars 10 µm at time 0 and at time 72 h with 3D zooms on outlined epiblasts. d. Quantification of the number of lumens in epiblast as a function of time with different initial cell numbers, 1, 2, 4, 8, 16 cells. Each point represents an individual cyst, while the dark line corresponds to the mean value, and the shaded region indicates the standard deviation. For a and c, the yellow line outlines the zone with single lumens. For both systems, the number of lumens increases as a function of time and with initial cell numbers. All cysts end up close to single lumens. Note that the timescales are different for the 3 systems indicated with the same colour code across the article (compare Fig. 2b, Fig. 2d and Fig. 1e).

Figure 3 - Rules of lumen nucleation in the 3 systems. The lumens are nucleated after cell division and after cells meet in MDCK spheres and pancreatic spheres but they form after about 5 cell divisions in epiblasts. a. Lumen nucleation per cell cycle as a function of initial cell numbers. The increase is linear for the 3 systems. MDCK and pancreatic spheres have the same slope whereas epiblasts have a slope 5 times lower. b. Snapshots of lumen nucleation in MDCK cysts. Top: Lumen formation after cell division in MDCK cysts (Movie 1) N=5, n=32. Bottom: Lumen formation after contacts between cells in MDCK cysts (Movie 2) N=4, n=10 (E-cadherin in green and Podocalyxin in red). Time relative to the junction formation set as time 0. Time in hh:mm. Scale bar 10 µm. c. Quantification of lumen appearance time after cell division or after cells meet. d. Snapshots of lumen nucleation in pancreatic spheres, Top: lumen formation after cell division, see also Movie 3. Bottom: lumen formation after two cells meet; see also Movie 4. Time relative to the junction formation set as time 0. Time in hh:mm. Scale bar 10 µm. e. Quantification of the lumen nucleation after cell division or after cells meet. f. Lumen nucleation in

519 epiblasts fixed at 8h, 16h, 24h, 32h, 40h and 48h after cell seeding, stained with DAPI in blue,
520 podoxalyxin in red and E-cadherin in green. g. Number of cells as a function of time. (N=2, n>10).
521
522
523 **Figure 4 - Rules of lumen fusion in the 3 systems.** MDCK and pancreatic spheres lumens fuse by
524 increasing the lumen index whereas epiblasts fuse by cell motion with low lumen index. a. Top: scheme
525 of lumen fusion corresponding to Phase II. Bottom: quantification for the speed of lumen fusion. The
526 plot represents lumen fusion per cell cycle as a function of initial cells number (mean value ± standard
527 error of the mean and the curve represent the fit of mean). Pancreatic spheres and epiblast display
528 faster lumen fusion than MDCK cysts. B. Lumen fusion across systems. Top: MDCK cyst (E-cadherin in
529 green and Podocalyxin in red, also see Movie 5). Middle: Pancreatic sphere (phase contrast images, also
530 see Movie 6). Bottom: epiblast (Sir-actin, also see movie 7). c-e. Comparison between lumen indices
531 (ratio of surface of lumen over the surface of cyst) for the three systems presented on panel b: MDCK
532 cyst (c), pancreatic sphere (d) and epiblast (e). For each system, the blue and black curves correspond to
533 individual lumen 1 and 2 on panel b. f-l. Characterization and comparison between cellular dynamics
534 and tissue morphology in MDCK cyst (top) and epiblast (bottom). f,i. Elongations of the cyst defined as
535 the ratio of long axis over short axis of the organoid as a function of time. g,h. Distance between the
536 center of cells and the center of cysts over time. During the fusion process, MDCK cells are at a constant
537 distance from the center of the cyst whereas epiblast cells move inwards. h,l. Single cells trajectories.
538 Time is indicated with color bar and red point indicate the last time point. Epiblast cells display
539 centripetal motion.

540 **Figure 5- Comparison between phenotypes and hydrostatic pressure in MDCK cysts, pancreatic**
541 **spheres and epiblasts**. a. Typical images of the 3 systems with readouts for E-cadherin in green and F-
542 actin in red. Scale bar 10 µm. b. Quantification of lumens index for the 3 systems. c. Comparison of E-
543 cadherin levels between the 3 systems defined as intensity of E-cadherin on the junction minus intensity
544 in the cytoplasm and normalised by the intensity of the background. **** corresponds to $p < 0.0001$.
545 (d) Measurements of hydrostatic pressure in MDCK cysts and epiblasts by laser cutting. Images show the
546 midplane cross-sections of cysts before and after laser cutting, with red segments indicating the
547 positions of cuts. (e) Estimation of hydrostatic pressure in the lumen using the Hagen-Poiseuille law (see
548 Methods). (f) Lumen volume changes over time following laser cutting. The dark line represents the
549 mean volume change, while the shaded region indicates the standard deviation. (g) Hydrostatic pressure
550 measurements show an average of 65 Pa in MDCK cysts and close to 0 Pa in epiblasts. Data are based on
551 three independent experiments (N=3), with 27 MDCK cysts (n=27) and 22 epiblast samples (n=22). Scale
552 bar: 10 µm.

553

554 **Figure 6 – Phase field model for the nucleation and fusion of lumens for the 3 systems.** a. The cells
555 increase in volume and divide when they reach a threshold volume or after a threshold time. A lumen is
556 formed after each division. The numerical cysts grow over time; see Movie 8 for typical numerical
557 evolution of cysts. b. The pressure Ksi and proliferation time are controlled and two conditions are
558 plotted as a function of numerical time. Each case corresponds qualitatively to each experimental
559 system, see also Movie 9 and Movie 10. c. Quantification of the number of lumens as a function of time.
560 The number of lumens increases and then decreases. These two subsequent phases are similar to the
561 experimental phases reported in Fig. 1 and in Fig. 2. d. Numerical lumen indices measured for the 2

conditions. Their dynamics are similar the 2 experimental dynamics reported in Fig. 4. e-i. e. Schematic showing the correlation between pressure and lumen formation time. Left panel: lumen formation is delayed in the absence of pressure; right panel: lumen nucleation can occur at the two-cell stage under applied pressure. f-h. Free energy dependency as a function of lumen radius for distinct hydrostatic pressure. (f) F(r, R_min) : (f) $\Delta p = 0$ [Pa] for N=2, 4, 8, 12. (g) $\Delta p = 30$ [Pa] for N=2, 4, 8, 12; and (h) $\Delta p = 100$ [Pa] for N=2, 4, 8, 12. Numerical parameters are $\gamma_A = 100\ [Pa \cdot \mu m]$, $\gamma_L = 100\ [Pa \cdot \mu m]$, $R_0 = 20\ [\mu m]$, $L = 40\ [\mu m]$, $L_0 = 38.5\ [\mu m]$, $k = 0.01$, $k_E = 0.02$ for all cases. For N=12 case, we assumed regular dodecahedron shape for calculation.

Figure 7 - Testing the fusion mechanisms with perturbation experiments on MDCK cysts. Increasing lumen size by injection or decreasing cells adhesion leads to faster to lumen fusion. a. Inflating MDCK spheres with micropipette. E-cadherin in green and podocalyxin in red and Dextran in Magenta. Scale bar: 20 µm. The inflation triggers the fusion between lumens. b. Effects of osmotic shock on MDCK cysts with multiple lumens. Experimental setup (top left): MDCK cysts were cultured for 1 day before being treated under control conditions or with D-mannitol. The culture duration is indicated in days. Representative images of cysts are shown at two time points: day 1 (top right) and day 3 (bottom left) for each condition. Cysts are stained for F-actin (magenta) to visualize structural changes. Scale bar: 10 µm. c. Statistical analysis based on three independent experiments (N=3), with 79 cysts in the control group (n=79) and 198 cysts in the D-mannitol-treated group (n=198). $p < 0.0001$. d. Decrease in cells adhesion leads to faster lumen fusion. Snapshot of timelapse with control (top) and EDTA + antibody block (bottom). E-cadherin in green and podocalyxin in red. Scale bar: 10 µm. e. Quantification of number of lumens after EDTA+antibody treatment. Two independent experiments. Statistical analyses: T test. **** $p < 0.0001$; ns, not significant. (n control=15; n EDTA=16). e-g. Decreasing cell adhesion by using MDCK E-cadherin KO. The comparisons between MDCK WT and E-cadherin KO cysts over time and initial cell number in d (top two rows: 8 cells, bottom two rows: 16 cells). f. Quantification of the number of lumens in WT and E-cadherin KO cysts as a function of time for the initial cell number 8 and 16 cells.

Figure 8: Perturbation of lumen fusion in the epiblast. (a) Representative images of the lumen fusion process in the epiblast. The top panel shows the control condition treated with DMSO, and the bottom panel shows the effect of blebbistatin treatment. Lumens are visualized with SiR-actin (gray). Scale bar: 5 µm. b-f. Numerical simulations for the fusion of epiblast-like cysts, see also Movie 11. b. Definition of parameters for the fusion of epiblast-like cysts. c. Fusion of two lumens in epiblast-like condition. d. The cell motions are tracked as well as the distance of cells with respect to the center of mass of the system (e) and the change in aspect ratio of the cysts (f). The numerical dynamics correspond closely to the experimental time evolution of the same measurements in epiblasts fusion, see Fig. 4j-l.

Figure 9 – Comparison of lumen nucleation and fusion in organoids with/without hydrostatic pressure. Row 1: Pancreatic spheres, MDCK cysts and epiblasts have two phases for the number of lumens as a function of time. **Row 2: Key differences in hydrostatic pressure observed between the three systems. Row 3:** Nucleation rules are similar for pancreatic spheres and MDCK cysts, lumens form after cell division and when two cells meet; in contrast, a minimum of about 10 cells are required for the lumen nucleation of lumens in epiblasts. **Row 4:** Lumens fusion are similar between pancreatic spheres and MDCK cysts but with distinct pumping rates. In pancreatic spheres, fast pumping leads the increase in lumen index and subsequent fusion; in MDCK cysts, lower increase in lumen index leads the fusion. In contrast, fusion occurs with centripetal cell motion in epiblasts with low lumen occupancies.

Extended Figures Captions

Extended figure 1: Diameter measurement: a. Middle plan of single cells for MDCK, mES, pancreatic progenitor from top to bottom labeled with Sir-actin. b. Diameter distribution: N=3, n=(MDCK), n=(mES), n= (pancreatic progenitor). Scale bar 5 µm. c. Selections of diameters for cavities for distinct cells.

Extended Figure 2: Examples of distributions for the number of lumens at the peak value at the end of Phase I (Left) and at the end of Phase II at the single lumen stage (Right).

Extended Figure 3: **Lumen nucleation in MDCK cysts and in epiblasts.** (a) Lumen formation is identified by the presence of a hole at the junction and the accumulation of the apical protein Podocalyxin. (b) Top two-panel row: epiblasts showing accumulation of Podocalyxin without lumen formation, as no hole is present at the junction. Bottom two-panel row: Lumen nucleation in epiblasts characterized by the accumulation of Podocalyxin and the presence of a hole at the junction. c. 3D visualization of cell counting in epiblasts. From left to right: 2D Cut: A cross-sectional view of the cells in 2D. 3D View with DAPI Staining: A 3D visualization highlighting nuclear structures with DAPI staining. Center of Cells in 3D: The central positions of cells in 3D space, marked in different colors to differentiate individual cells. Merged View: A composite image that integrates the 3D DAPI visualization with the 3D cell centers. Scale bar: 10 µm.

Extended Figure 4*:* Lumen fusion dynamics across different systems. (a) Representative examples of lumen fusion in MDCK cysts, pancreatic spheres, and epiblasts, along with quantification of the lumen index. Lumens with low and high lumen index are shown in blue and black, respectively, while the sum is indicated in red. MDCK cysts are labeled with E-cadherin (green) and Podocalyxin (red), while pancreatic spheres and epiblasts are visualized using SiR-actin (gray). Additional examples of lumen fusion are also shown. (b) Quantification of lumen index in another set of examples across the three systems. (c) Mean lumen index for each system, represented by the dark line, with the shaded region indicating the standard deviation (N=3, n=3). Scale bar: 10 µm.

Extended Figure 5: Adhesion is different between epithelial cysts. (a) Immuno-staining of wild type MDCK and MDCK cells overexpressing E-cadherin, scale bar 20 µm. Cyst are stained for F-actin (magenta) and nucleus in cyan. (b) Western blots for E-cadherin comparing wild type MDCK cells, MDCK cells overexpressing E-cadherins, and (c) epiblasts. (d) Micropipette inflation experiments on MDCK cysts (left) and epiblasts (right) (see Mukenhirn et al, 2024[22]).

Extended Figure 6: Association between lumen index and hydrostatic pressure. (a) Time-lapse images showing drainage triggered by a local laser cut in MDCK cysts, with the midplane captured before and after the cut. The positions of the cuts are marked by red segments. Two representative examples are shown, with time indicated in seconds (s). Scale bar: 10 µm. (see Mukenhirn et al., 2024[22] for details). (b) Relationship between hydrostatic pressure and lumen occupancy in MDCK cysts. (c) Laser-induced drainage experiment demonstrating changes in cyst midplane over time, with the cut positions indicated by red lines. The volume of each lumen is monitored throughout the experiment (d) Volume changes in lumens over time, where different colors represent individual cysts. Smaller

lumens are depicted by blue circles, and larger lumens by black squares. (e) Corresponding hydrostatic pressure differences for each experiment, with the color coding consistent with panel (d).

Extended Figure 7: Surface tension measurement of MDCK cysts with single and multiple lumens. (a) Brightfield Images: Representative brightfield images show MDCK cysts undergoing surface tension measurements, highlighting cysts with multiple lumens (top panel) and a single lumen (bottom panel). Scale bar: 20 µm. (b) Box Plot Analysis: Data are presented as mean ± standard deviation (s.d.) with individual data points overlaid, providing a view of both central tendency and data variability.

Extended Figure 8: Micropipette inflation swelling experiments on MDCK cysts with two lumens. The left two panels show the cysts before injection, and the right two panels show the cysts after injection. Each row represents an individual example. Cysts are labeled with E-cadherin (green), Podocalyxin (red), and Dextran (magenta). The inflation procedure triggers lumen fusion. Scale bar: 10 µm.

Extended Figure 9: Micropipette inflation assay in epiblasts and MDCK-II cysts. Micropipette inflation swelling experiments on epiblasts with two lumens. Top panels show the condition before injection, and bottom panels show after injection, with three images corresponding to (left to right): dextran staining, SiR-actin + dextran overlay, and transmission light microscopy. Scale bar: 10 µm.

Extended Figure 10: Comparison between MDCK wild type, ZO1/ZO2 KO cysts and epiblasts. a. Cell-cell contacts and lumens are stained with E-cadherin (in green) and F-actin (in red), scale bar: 5 µm. Note the low lumen index in epiblasts and MDCK ZO1/ZO2 KO cysts. b-d. Comparison between inflation response (to be completed). B. Images are shown before and after inflation. c. Change fold in the lumen volume for each system, statistical test. d. Change in cell height for each system[22].

Extended Figure 11: Lumen fusion dynamics in MDCK WT and ZO-KO cysts. (a, b) ZO-KO cyst have faster lumen fusion than WT in MDCK cysts with controlled initial cell number. Dynamics of MDCK WT cysts (a) and ZO-KO cyst (b) with readouts of E-cadherin in green and Podocalyxin in red. The yellow line outlines zones with a single lumen (8 cells WT=15; 16 cells WT=16; 8 cells ZO-KO=13; 16 cells ZO-KO=16). (c) Lumen fusion comparison between MDCK WT cysts, ZO-KO cysts, and epiblasts, showing that ZO-KO mutants exhibit fusion behavior similar to epiblasts. MDCK WT and ZO-KO cysts are labeled with Podocalyxin (red) and E-cadherin (green), while epiblasts are stained with SiR-actin (gray). Scale bar: 10 µm.

References.

1. Zhu, M. & Zernicka-Goetz, M. Principles of Self-Organization of the Mammalian Embryo. *Cell* **183**, 1467–1478 (2020).

2. Wennekamp, S., Mesecke, S., Nédélec, F. & Hiiragi, T. A self-organization framework for symmetry breaking in the mammalian embryo. *Nat Rev Mol Cell Biol* **14**, 452–459 (2013).
3. Hannezo, E. & Simons, B. D. Multiscale dynamics of branching morphogenesis. *Current Opinion in Cell Biology* **60**, 99–105 (2019).
4. Martín-Belmonte, F. *et al.* Cell-Polarity Dynamics Controls the Mechanism of Lumen Formation in Epithelial Morphogenesis. *Current Biology* **18**, 507–513 (2008).
5. Strilić, B. *et al.* The Molecular Basis of Vascular Lumen Formation in the Developing Mouse Aorta. *Developmental Cell* **17**, 505–515 (2009).
6. Mangan, A. J. *et al.* Cingulin and actin mediate midbody-dependent apical lumen formation during polarization of epithelial cells. *Nat Commun* **7**, 12426 (2016).
7. Sigurbjörnsdóttir, S., Mathew, R. & Leptin, M. Molecular mechanisms of de novo lumen formation. *Nat Rev Mol Cell Biol* **15**, 665–676 (2014).
8. Datta, A., Bryant, D. M. & Mostov, K. E. Molecular regulation of lumen morphogenesis. *Curr Biol* **21**, R126-136 (2011).
9. Mailleux, A. A., Overholtzer, M. & Brugge, J. S. Lumen formation during mammary epithelial morphogenesis: insights from in vitro and in vivo models. *Cell Cycle* **7**, 57–62 (2008).
10. Dasgupta, S., Gupta, K., Zhang, Y., Viasnoff, V. & Prost, J. Physics of lumen growth. *Proc Natl Acad Sci U S A* **115**, E4751–E4757 (2018).
11. Torres-Sánchez, A., Kerr Winter, M. & Salbreux, G. Tissue hydraulics: Physics of lumen formation and interaction. *Cells & Development* **168**, 203724 (2021).
12. Dumortier, J. G. *et al.* Hydraulic fracturing and active coarsening position the lumen of the mouse blastocyst. *Science* **365**, 465–468 (2019).
13. Li, Q. *et al.* Extracellular matrix scaffolding guides lumen elongation by inducing anisotropic intercellular mechanical tension. *Nat Cell Biol* **18**, 311–318 (2016).

14. Ryan, A. Q., Chan, C. J., Graner, F. & Hiiragi, T. Lumen Expansion Facilitates Epiblast-Primitive Endoderm Fate Specification during Mouse Blastocyst Formation. *Developmental Cell* **51**, 684-697.e4 (2019).

15. Indana, D. *et al.* Lumen expansion is initially driven by apical actin polymerization followed by osmotic pressure in a human epiblast model. *Cell Stem Cell* **31**, 640-656.e8 (2024).

16. Chan, C. J. *et al.* Hydraulic control of mammalian embryo size and cell fate. *Nature* **571**, 112–116 (2019).

17. Villasenor, A., Chong, D. C., Henkemeyer, M. & Cleaver, O. Epithelial dynamics of pancreatic branching morphogenesis. *Development* **137**, 4295–4305 (2010).

18. Kesavan, G. *et al.* Cdc42-Mediated Tubulogenesis Controls Cell Specification. *Cell* **139**, 791–801 (2009).

19. Chan, C. J. & Hiiragi, T. Integration of luminal pressure and signalling in tissue self-organization. *Development* **147**, dev181297 (2020).

20. Bhat, A. *et al.* How to orient cells in microcavities for high resolution imaging of cytokinesis and lumen formation. in *Methods in Cell Biology* vol. 158 25–41 (Elsevier, 2020).

21. Taniguchi, K. *et al.* Lumen Formation Is an Intrinsic Property of Isolated Human Pluripotent Stem Cells. *Stem Cell Reports* **5**, 954–962 (2015).

22. Mukenhirn, M. *et al.* Tight junctions control lumen morphology via hydrostatic pressure and junctional tension. *Developmental Cell* S1534580724004568 (2024) doi:10.1016/j.devcel.2024.07.016.

23. Lee, B. H. *et al.* Control of lumen geometry and topology by the interplay between pressure and cell proliferation rate in pancreatic organoids. Preprint at https://doi.org/10.1101/2024.05.29.596462 (2024).

24. Nonomura, M. Study on Multicellular Systems Using a Phase Field Model. *PLoS ONE* **7**, e33501 (2012).

25. Akiyama, M., Nonomura, M., Tero, A. & Kobayashi, R. Numerical study on spindle positioning using phase field method. *Phys. Biol.* **16**, 016005 (2018).

26. Tanida, S. *et al. The Interplay between Lumen Pressure and Cell Proliferation Determines Organoid Morphology in a Multicellular Phase Field Model*. http://biorxiv.org/lookup/doi/10.1101/2023.08.17.553655 (2023) doi:10.1101/2023.08.17.553655.

27. Harris, A. R., Daeden, A. & Charras, G. T. Formation of adherens junctions leads to the emergence of a tissue-level tension in epithelial monolayers. *Journal of Cell Science* jcs.142349 (2014) doi:10.1242/jcs.142349.

28. Comelles, J. *et al.* Epithelial colonies in vitro elongate through collective effects. *eLife* **10**, e57730 (2021).

29. Otani, T. *et al.* Claudins and JAM-A coordinately regulate tight junction formation and epithelial polarity. *Journal of Cell Biology* **218**, 3372–3396 (2019).

30. Li, D., Mangan, A., Cicchini, L., Margolis, B. & Prekeris, R. FIP 5 phosphorylation during mitosis regulates apical trafficking and lumenogenesis. *EMBO Rep* **15**, 428–437 (2014).

31. Zieger, E. *et al.* Midbody-Localized Aquaporin Mediates Intercellular Lumen Expansion During Early Cleavage of an Invasive Freshwater Bivalve. *Front. Cell Dev. Biol.* **10**, 894434 (2022).

32. Zhang, Y. *et al.* Biomimetic niches reveal the minimal cues to trigger apical lumen formation in single hepatocytes. *Nat. Mater.* **19**, 1026–1035 (2020).

33. Shahbazi, M. N. *et al.* Pluripotent state transitions coordinate morphogenesis in mouse and human embryos. *Nature* **552**, 239–243 (2017).

34. Kim, Y. S. *et al.* Deciphering epiblast lumenogenesis reveals proamniotic cavity control of embryo growth and patterning. *Sci. Adv.* **7**, eabe1640 (2021).

749 35. Alvers, A. L., Ryan, S., Scherz, P. J., Huisken, J. & Bagnat, M. Single continuous lumen formation
750 in the zebrafish gut is mediated by *smoothened* -dependent tissue remodeling. *Development* **141**,
751 1110–1119 (2014).
752 36. Bagnat, M., Cheung, I. D., Mostov, K. E. & Stainier, D. Y. R. Genetic control of single lumen
753 formation in the zebrafish gut. *Nat Cell Biol* **9**, 954–960 (2007).
754 37. Carleton, A. E., Duncan, M. C. & Taniguchi, K. Human epiblast lumenogenesis: From a cell
755 aggregate to a lumenal cyst. *Seminars in Cell & Developmental Biology* **131**, 117–123 (2022).
756 38. Dahl-Jensen, S. B. *et al.* Deconstructing the principles of ductal network formation in the
757 pancreas. *PLoS Biol* **16**, e2002842 (2018).
758 39. Gonay, L. *et al.* Modelling of Epithelial Growth, Fission and Lumen Formation During Embryonic
759 Thyroid Development: A Combination of Computational and Experimental Approaches. *Front.*
760 *Endocrinol.* **12**, 655862 (2021).
761 40. Bedzhov, I. & Zernicka-Goetz, M. Self-Organizing Properties of Mouse Pluripotent Cells Initiate
762 Morphogenesis upon Implantation. *Cell* **156**, 1032–1044 (2014).
763 41. Noor, N. *et al.* 3D Printing of Personalized Thick and Perfusable Cardiac Patches and Hearts.
764 *Advanced Science* **6**, 1900344 (2019).
765 42. Jorgensen, A. M. *et al.* Multicellular bioprinted skin facilitates human-like skin architecture in
766 vivo. *Sci. Transl. Med.* **15**, eadf7547 (2023).
767 43. Martin-Lemaitre, C., Alcheikh, Y., Naumann, R. & Honigmann, A. *Optimization of Mouse*
768 *Embryonic Stem Cell Culture for Organoid and Chimeric Mice Production*.
769 http://biorxiv.org/lookup/doi/10.1101/2020.03.13.990135 (2020) doi:10.1101/2020.03.13.990135.
770 44. Greggio, C., De Franceschi, F., Figueiredo-Larsen, M. & Grapin-Botton, A. In Vitro Pancreas
771 Organogenesis from Dispersed Mouse Embryonic Progenitors. *JoVE* 51725 (2014) doi:10.3791/51725.

45. Lu, L. *et al. Polarity-Driven Three-Dimensional Spontaneous Rotation of a Cell Doublet*. http://biorxiv.org/lookup/doi/10.1101/2022.12.21.521355 (2022) doi:10.1101/2022.12.21.521355.

46. Balasubramaniam, L. *et al.* Investigating the nature of active forces in tissues reveals how contractile cells can form extensile monolayers. *Nat. Mater.* **20**, 1156–1166 (2021).

47. Wollrab, V., Thiagarajan, R., Wald, A., Kruse, K. & Riveline, D. Still and rotating myosin clusters determine cytokinetic ring constriction. *Nat Commun* **7**, 11860 (2016).

48. Greggio, C. *et al.* Artificial three-dimensional niches deconstruct pancreas development *in vitro*. *Development* **140**, 4452–4462 (2013).

49. Guevorkian, K. & Maître, J.-L. Micropipette aspiration. in *Methods in Cell Biology* vol. 139 187–201 (Elsevier, 2017).

50. Ahrens, J., Geveci, B. & Law, C. ParaView: An End-User Tool for Large-Data Visualization. in *Visualization Handbook* 717–731 (Elsevier, 2005). doi:10.1016/B978-012387582-2/50038-1.

51. Olsson, E. & Kreiss, G. A conservative level set method for two phase flow. *Journal of Computational Physics* **210**, 225–246 (2005).

52. Badillo, A. Quantitative phase-field modeling for boiling phenomena. *Phys. Rev. E* **86**, 041603 (2012).

Figure 1

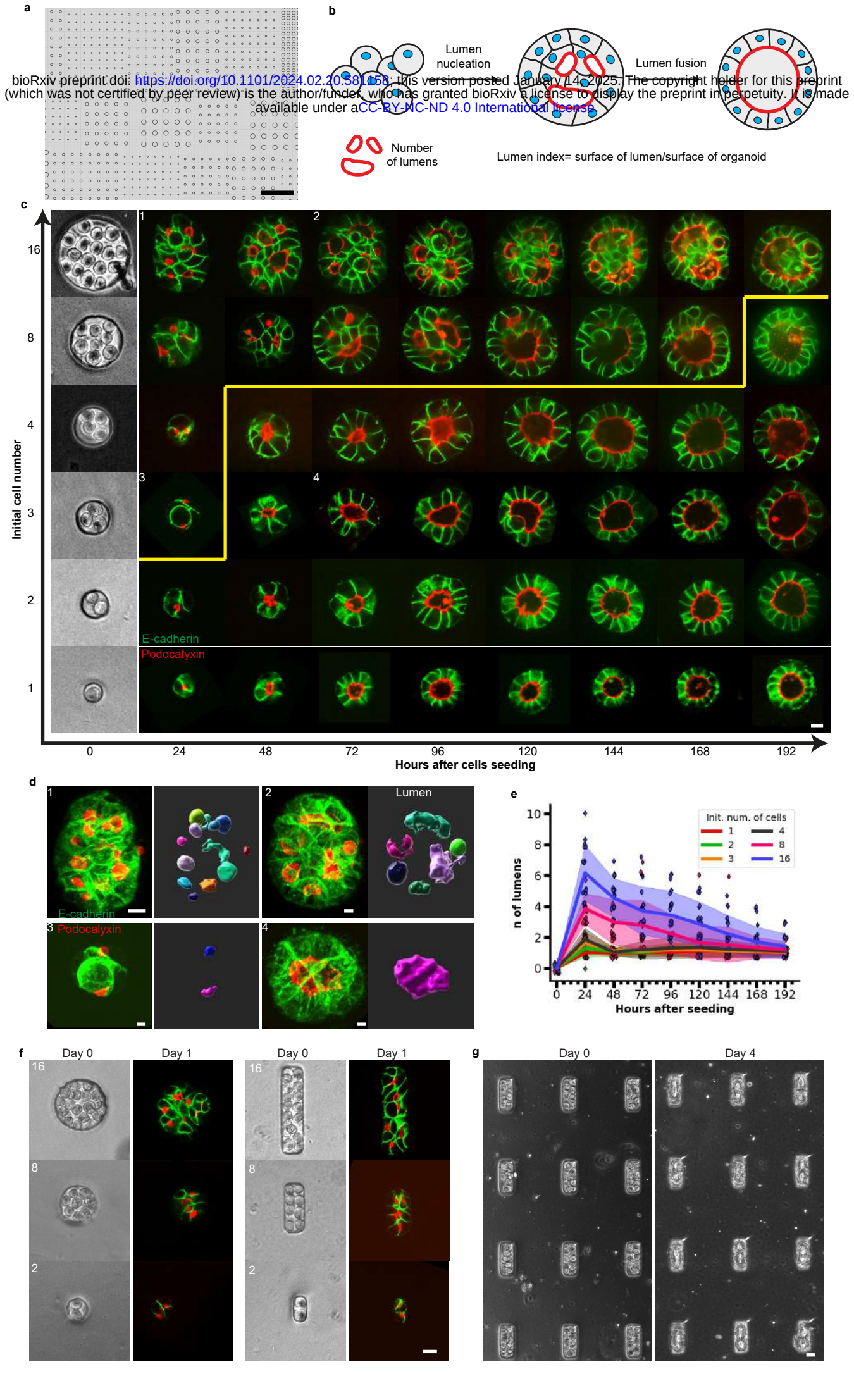

Figure 2

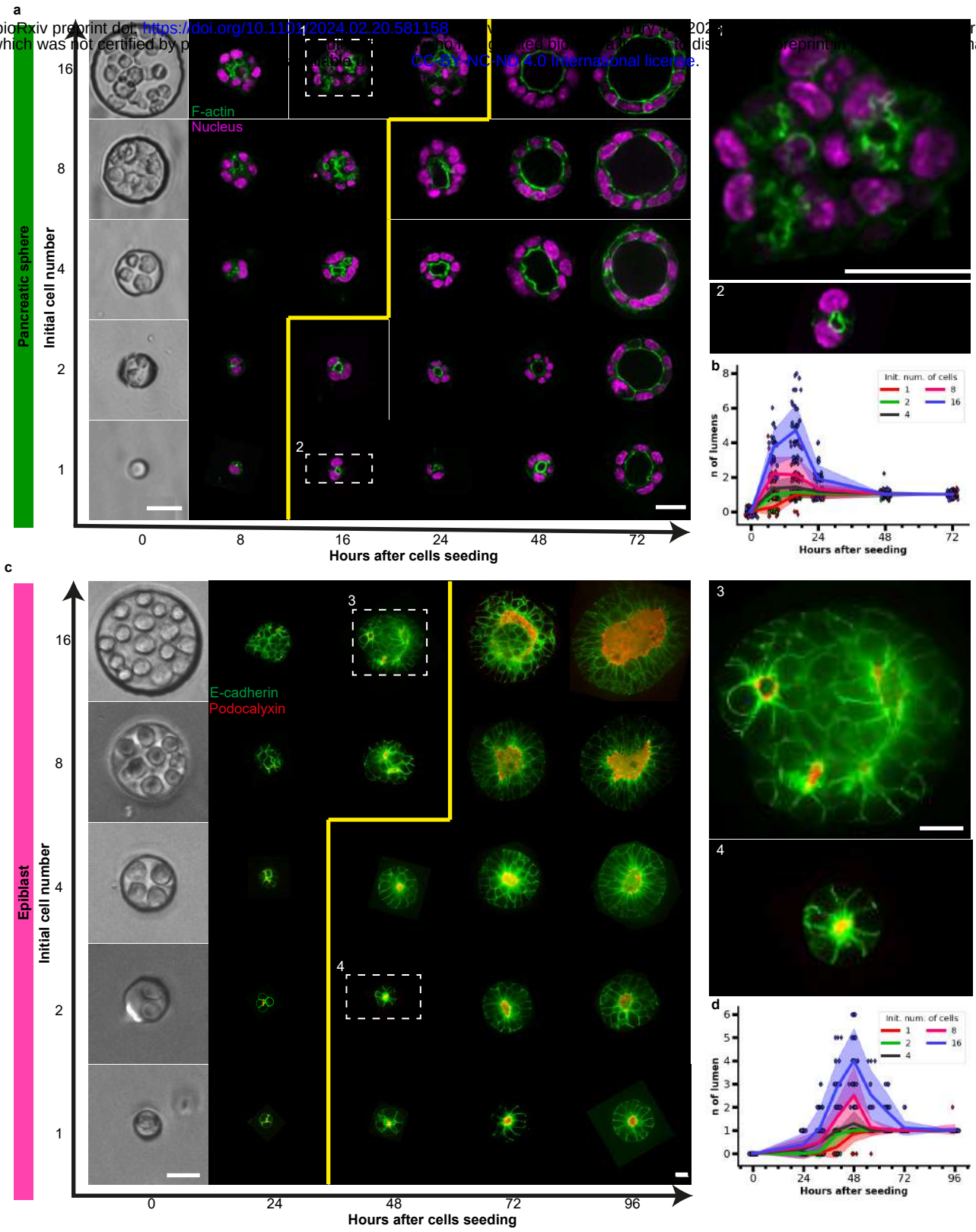

Figure 3

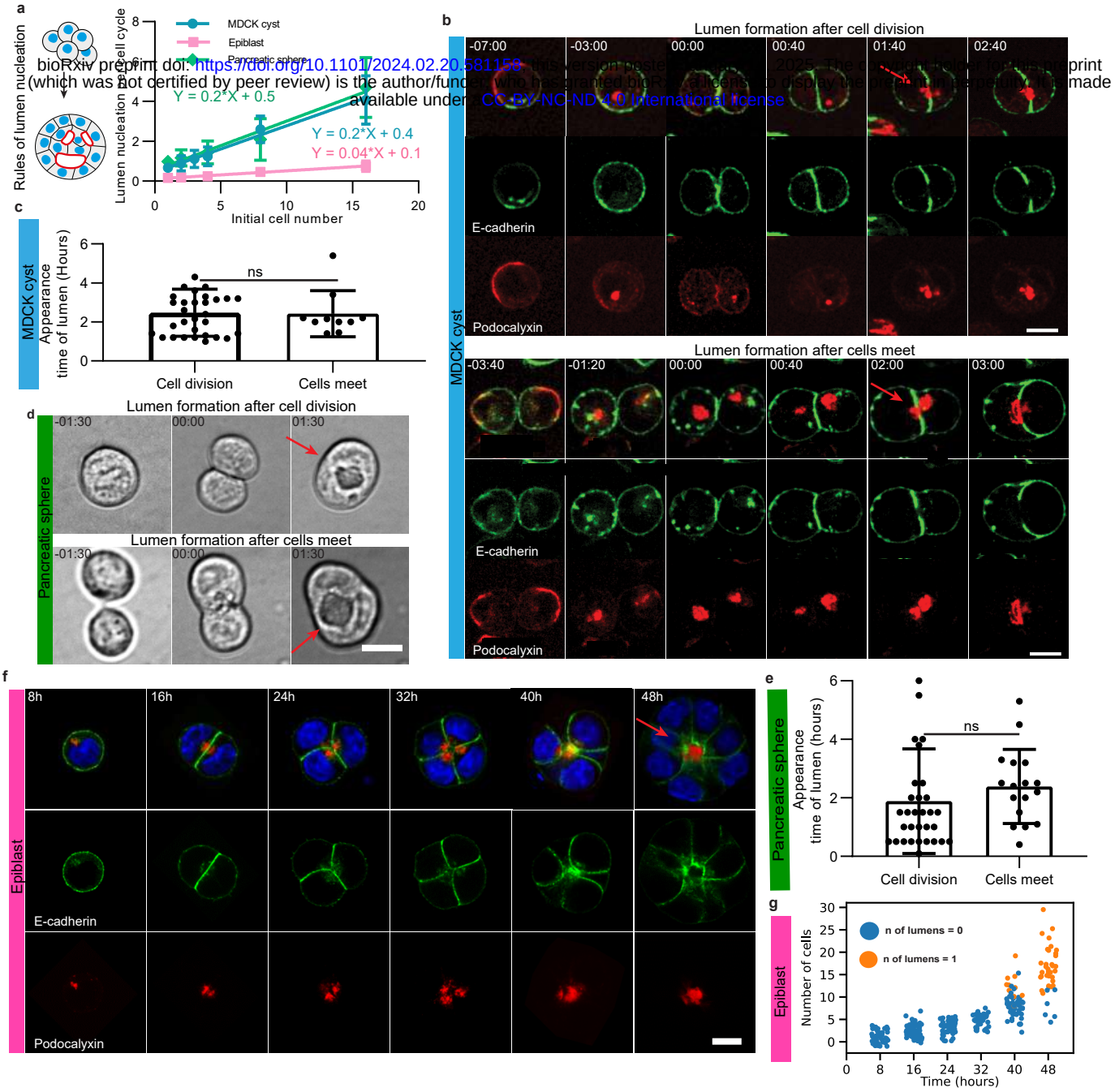

Figure 4

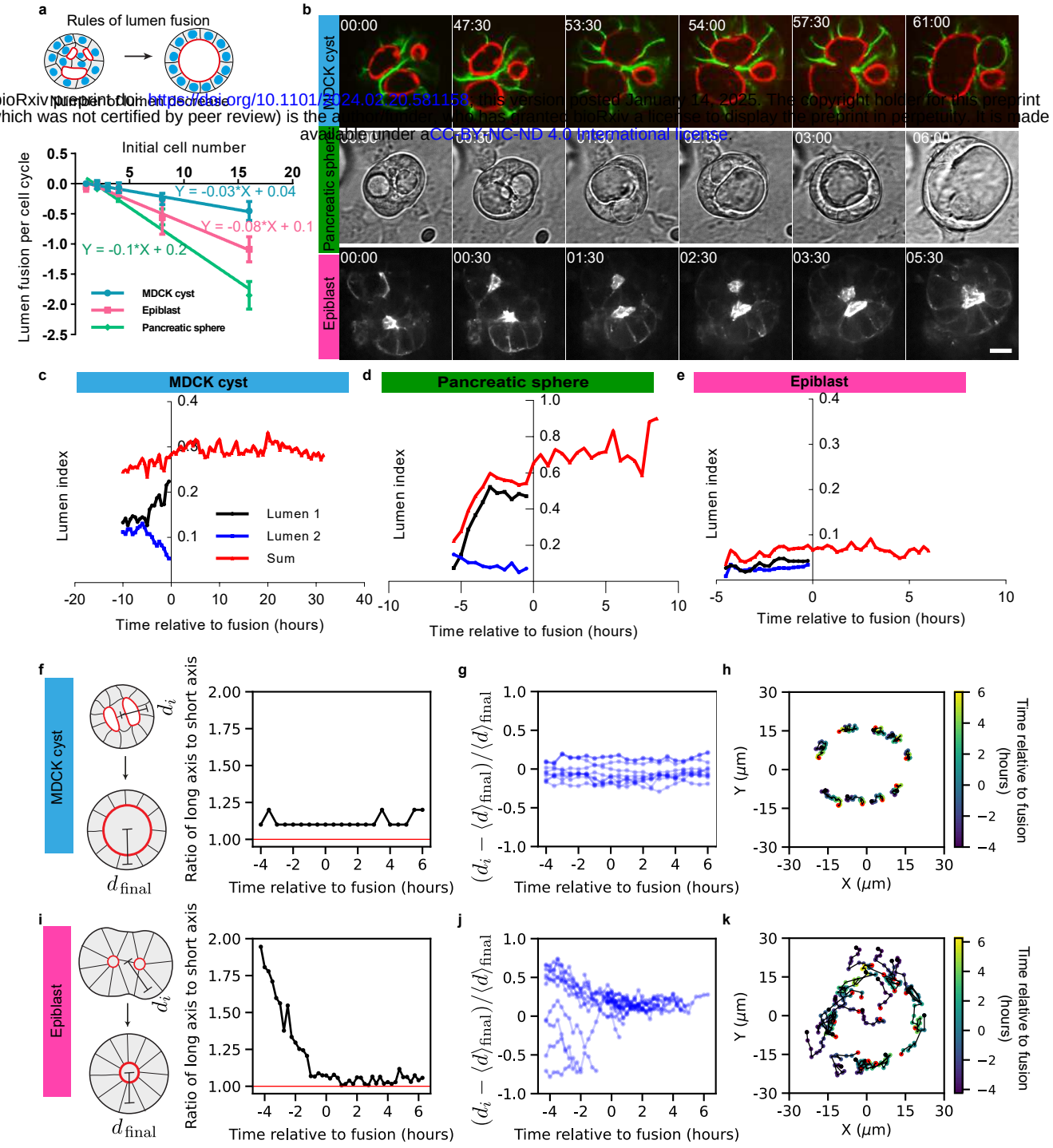

Figure 5

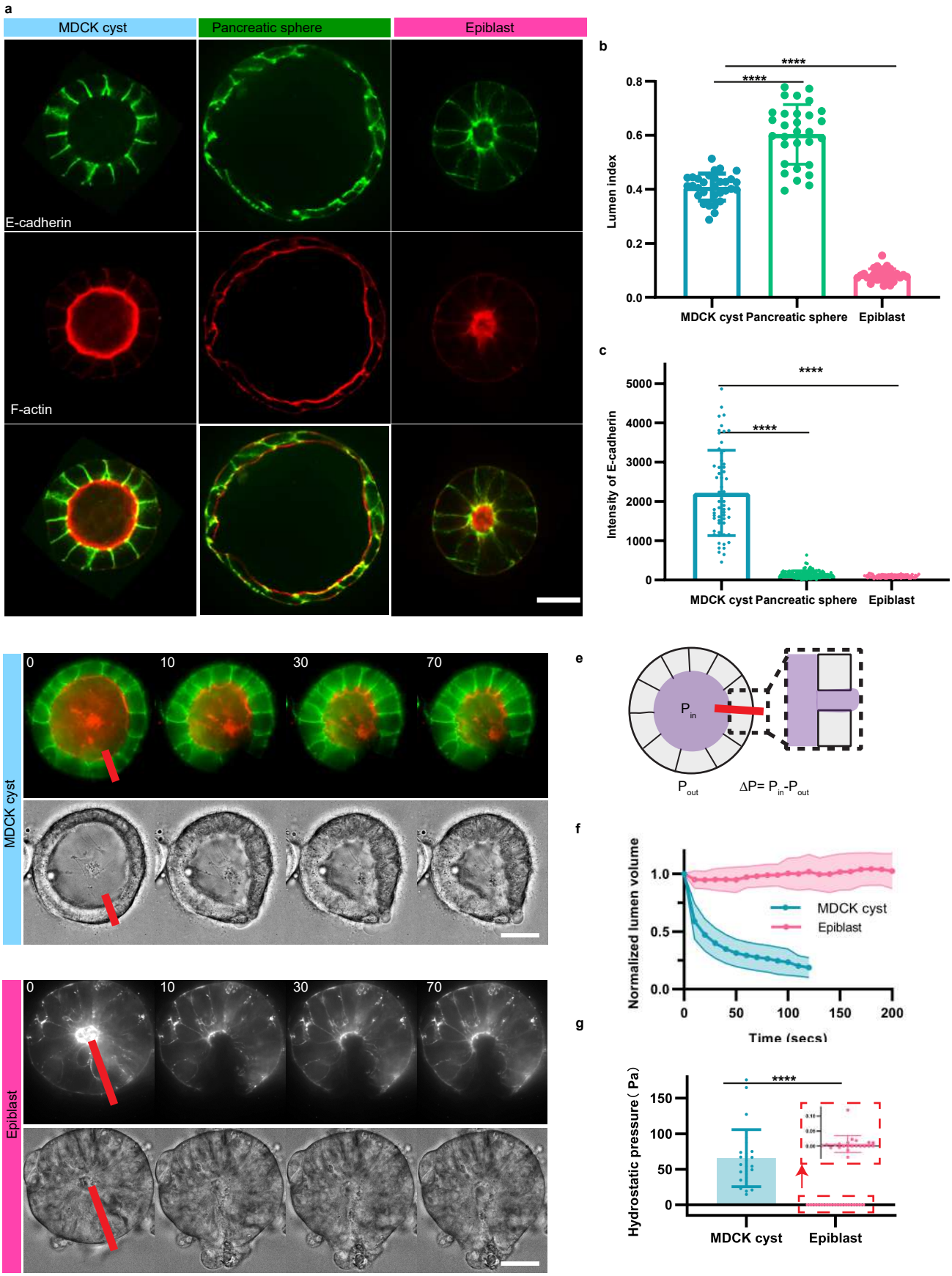
a
MDCK cyst
Pancreatic sphere
Epiblast
E-cadherin
F-actin
b
Lumen index
0.0
0.2
0.4
0.6
0.8
****
****
MDCK cyst
Pancreatic sphere
Epiblast
c
Intensity of E-cadherin
0
1000
2000
3000
4000
5000
****
****
MDCK cyst
Pancreatic sphere
Epiblast
d
MDCK cyst
Epiblast
0
10
30
70
e
P in
P out
ΔP= P in -P out
f
Normalized lumen volume
0.0
0.5
1.0
0
50
100
150
200
Time (secs)
MDCK cyst
Epiblast
g
Hydrostatic pressure (Pa)
0
50
100
150
****
MDCK cyst
Epiblast

Figure 6

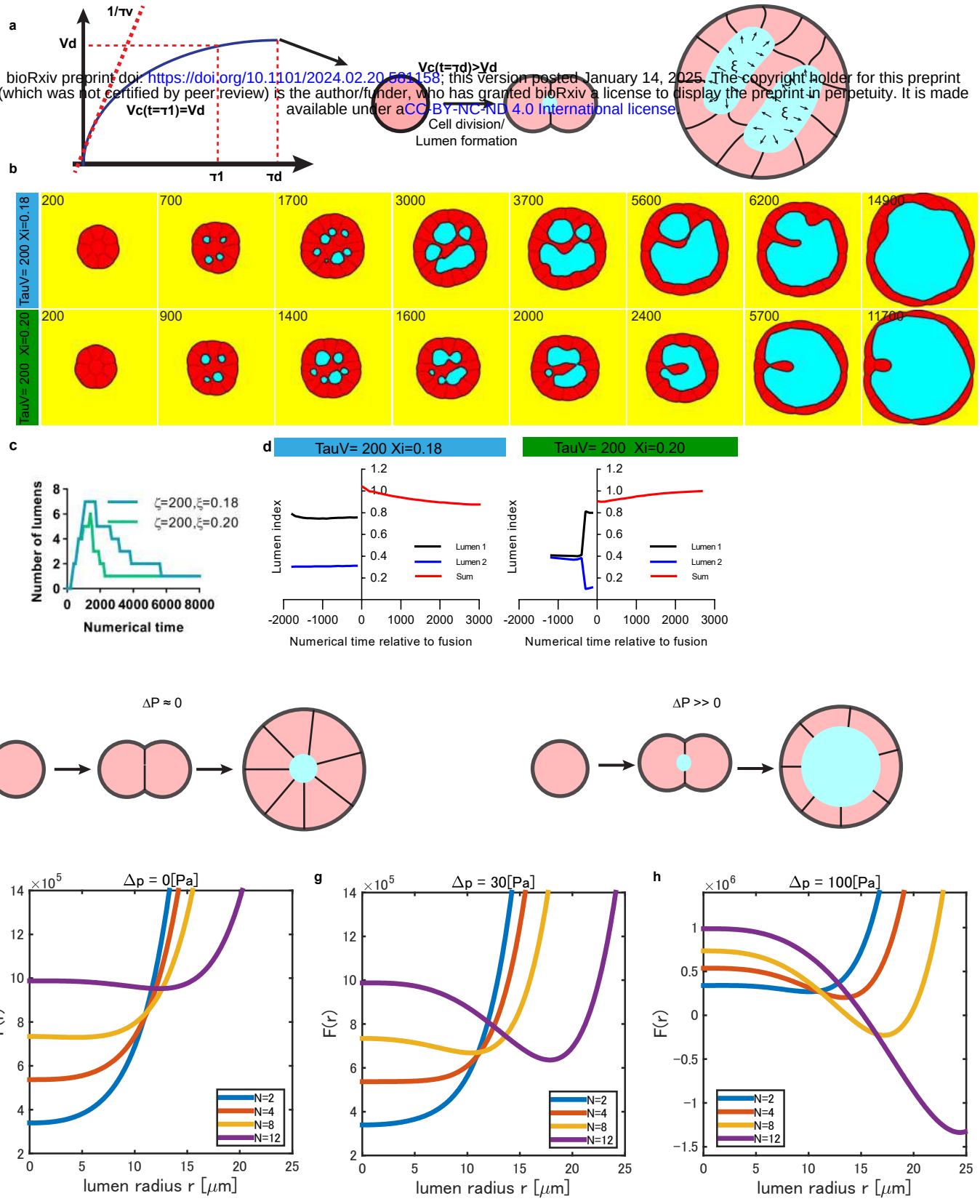

Figure 7

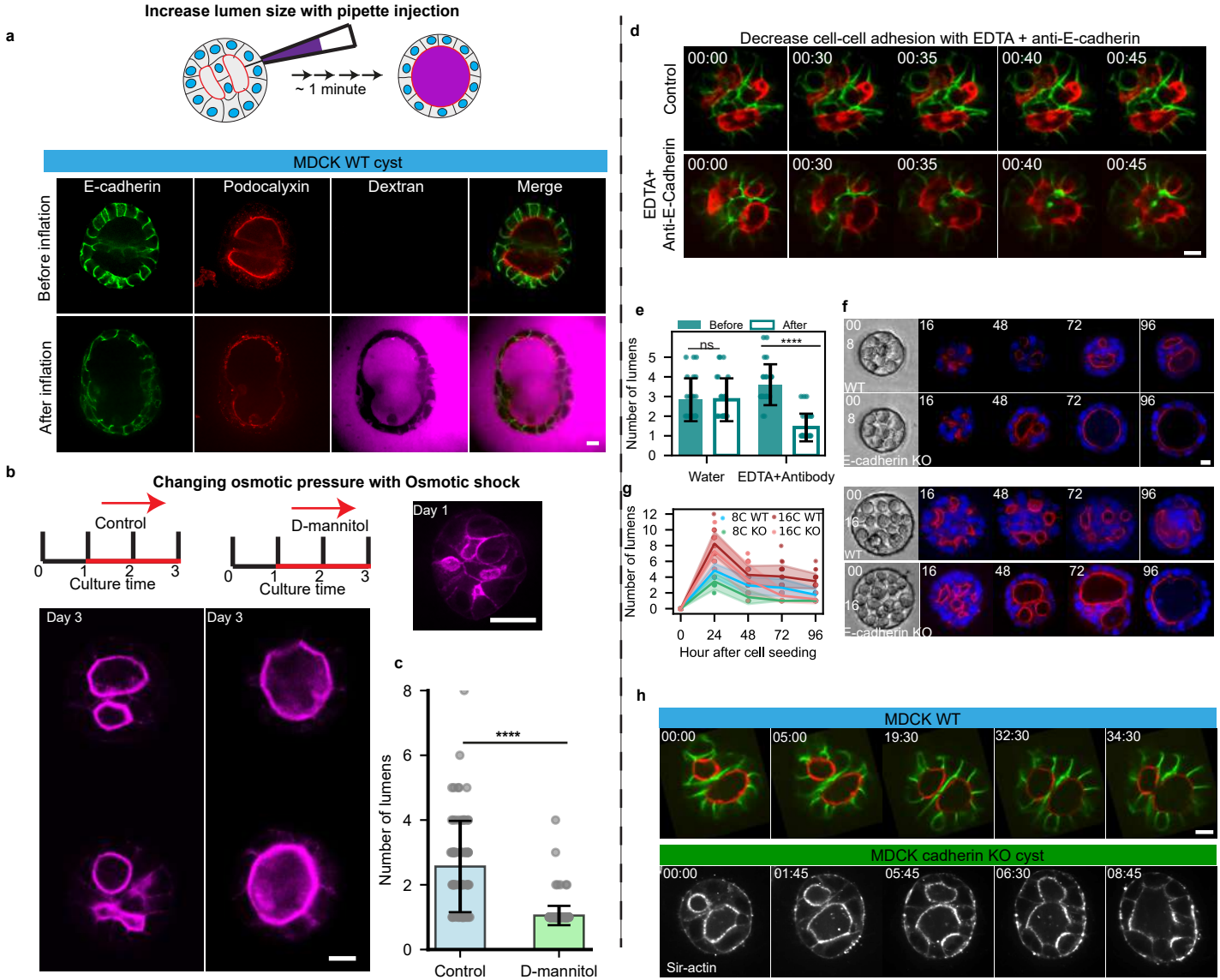
a
Increase lumen size with pipette injection
~ 1 minute
MDCK WT cyst
E-cadherin
Podocalyxin
Dextran
Merge
Before inflation
After inflation
b
Changing osmotic pressure with Osmotic shock
Control
D-mannitol
0 1 2 3
Culture time
Day 1
Day 3
Day 3
c
Number of lumens
****
Control
D-mannitol
d
Decrease cell-cell adhesion with EDTA + anti-E-cadherin
Control
EDTA+ Anti-E-Cadherin
00:00
00:30
00:35
00:40
00:45
e
Before
After
ns
****
Number of lumens
Water
EDTA+Antibody
f
WT
E-cadherin KO
00
8
16
48
72
96
g
8C WT
16C WT
8C KO
16C KO
Number of lumens
Hour after cell seeding
h
MDCK WT
00:00
05:00
19:30
32:30
34:30
MDCK cadherin KO cyst
00:00
01:45
05:45
06:30
08:45
Sir-actin

Figure 8

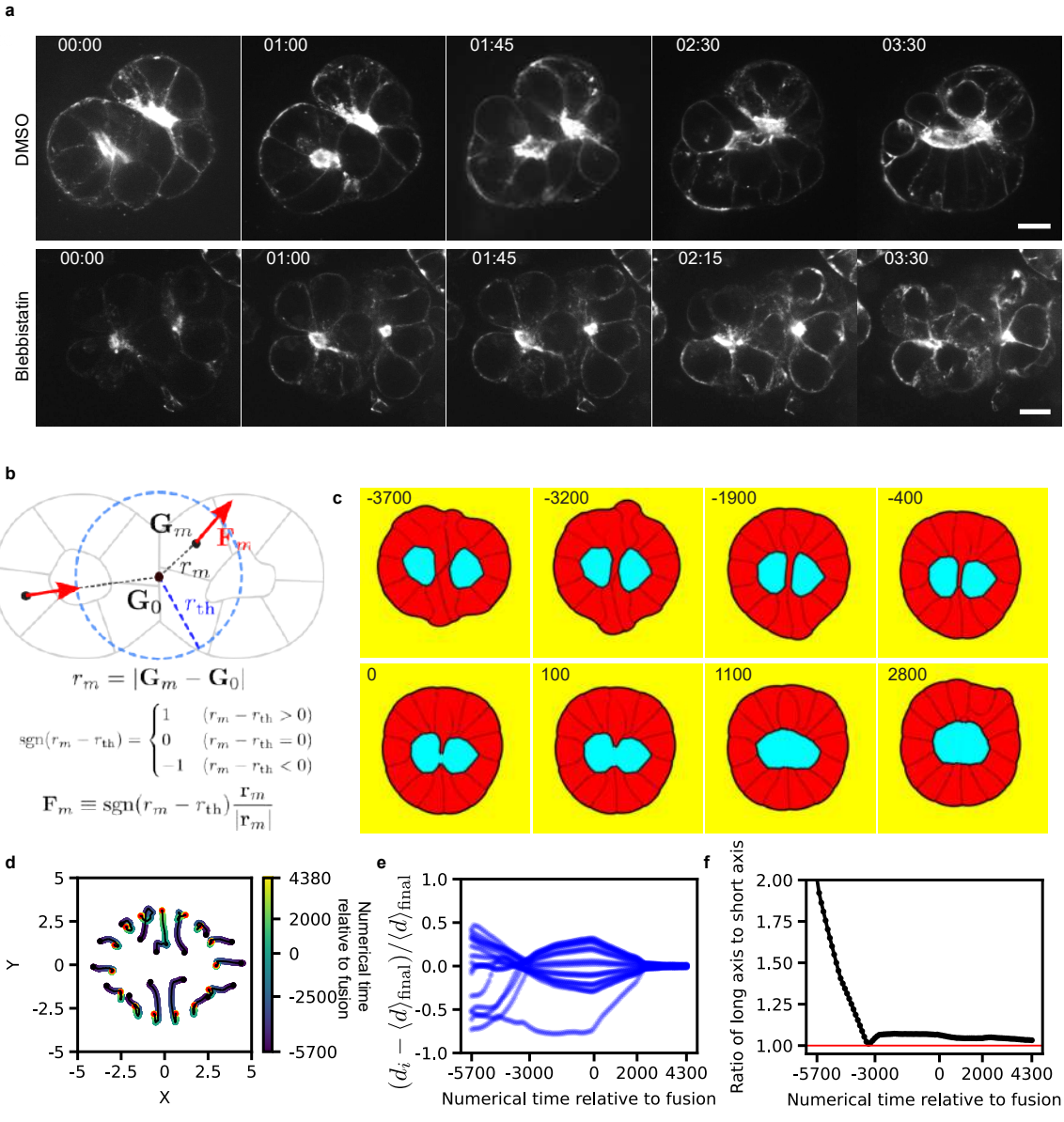
a
DMSO
00:00
01:00
01:45
02:30
03:30
Blebbistatin
00:00
01:00
01:45
02:15
03:30
b
$\mathbf{G}_m$
$\mathbf{F}_m$
r_m
$\mathbf{G}_0$
$r_{\rm th}$
$r_m = |\mathbf{G}_m - \mathbf{G}_0|$
$\mathrm{sgn}(r_m - r_{\rm th}) = \begin{cases} 1 & (r_m - r_{\rm th} > 0) \\ 0 & (r_m - r_{\rm th} = 0) \\ -1 & (r_m - r_{\rm th} < 0) \end{cases}$
$\mathbf{F}_m \equiv \mathrm{sgn}(r_m - r_{\rm th}) \frac{\mathbf{r}_m}{|\mathbf{r}_m|}$
c
-3700
-3200
-1900
-400
0
100
1100
2800
d
Y
X
Numerical time relative to fusion
4380
2000
0
-2500
-5700
e
$(d_i - \langle d \rangle_{\rm final}) / \langle d \rangle_{\rm final}$
Numerical time relative to fusion
f
Ratio of long axis to short axis
Numerical time relative to fusion

Figure 9

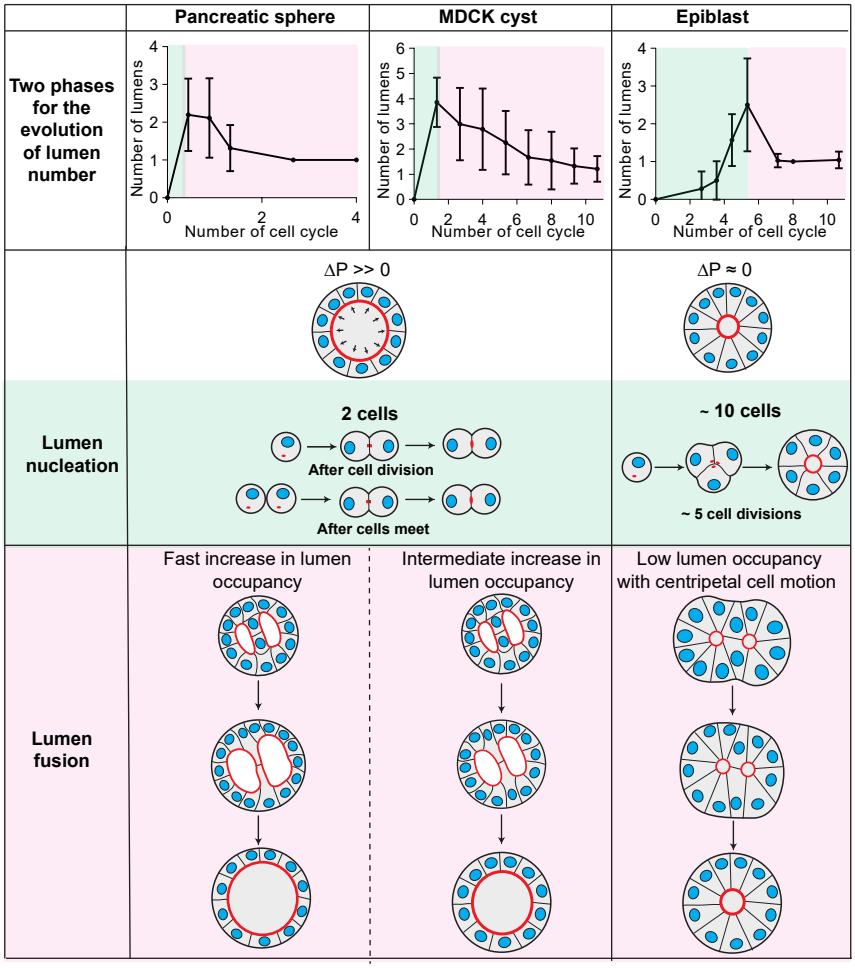

Extended Figure 1

a

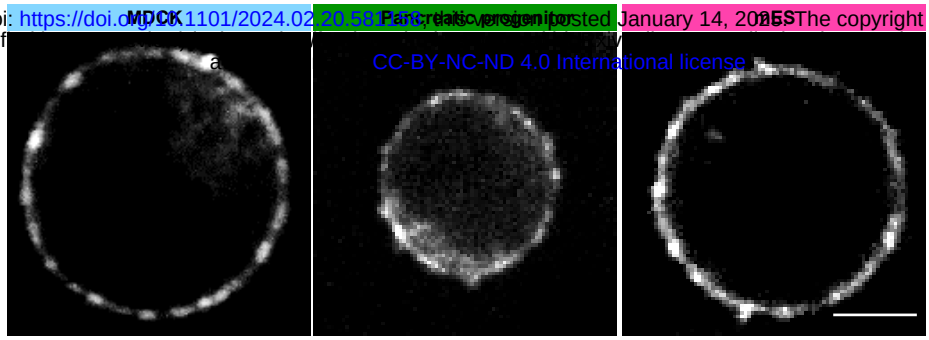

b

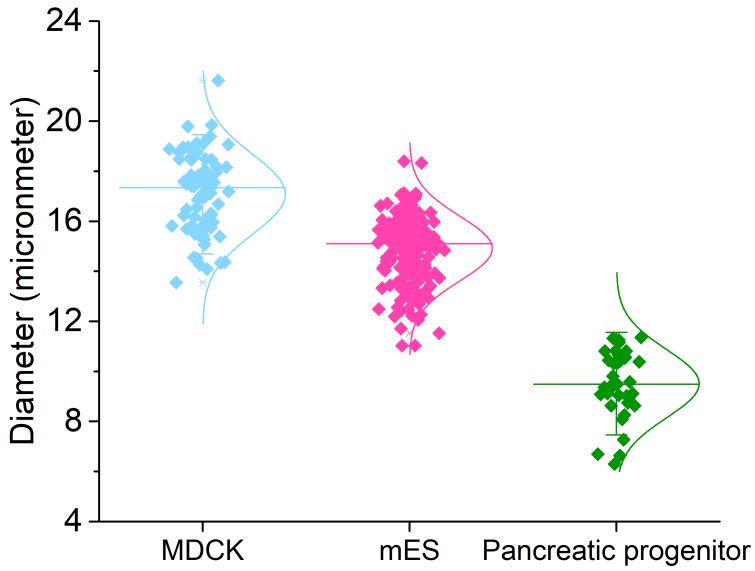

c

Initial cell numbers	MDCK cyst	Pancreatic sphere	Epiblast
	Diameter of cavities (μm)		
1	17.5	10	15
2	25	14	21
3	30	-	-
4	35	20	30
8	50	30	42
16	70	40	60

Extended Figure 2

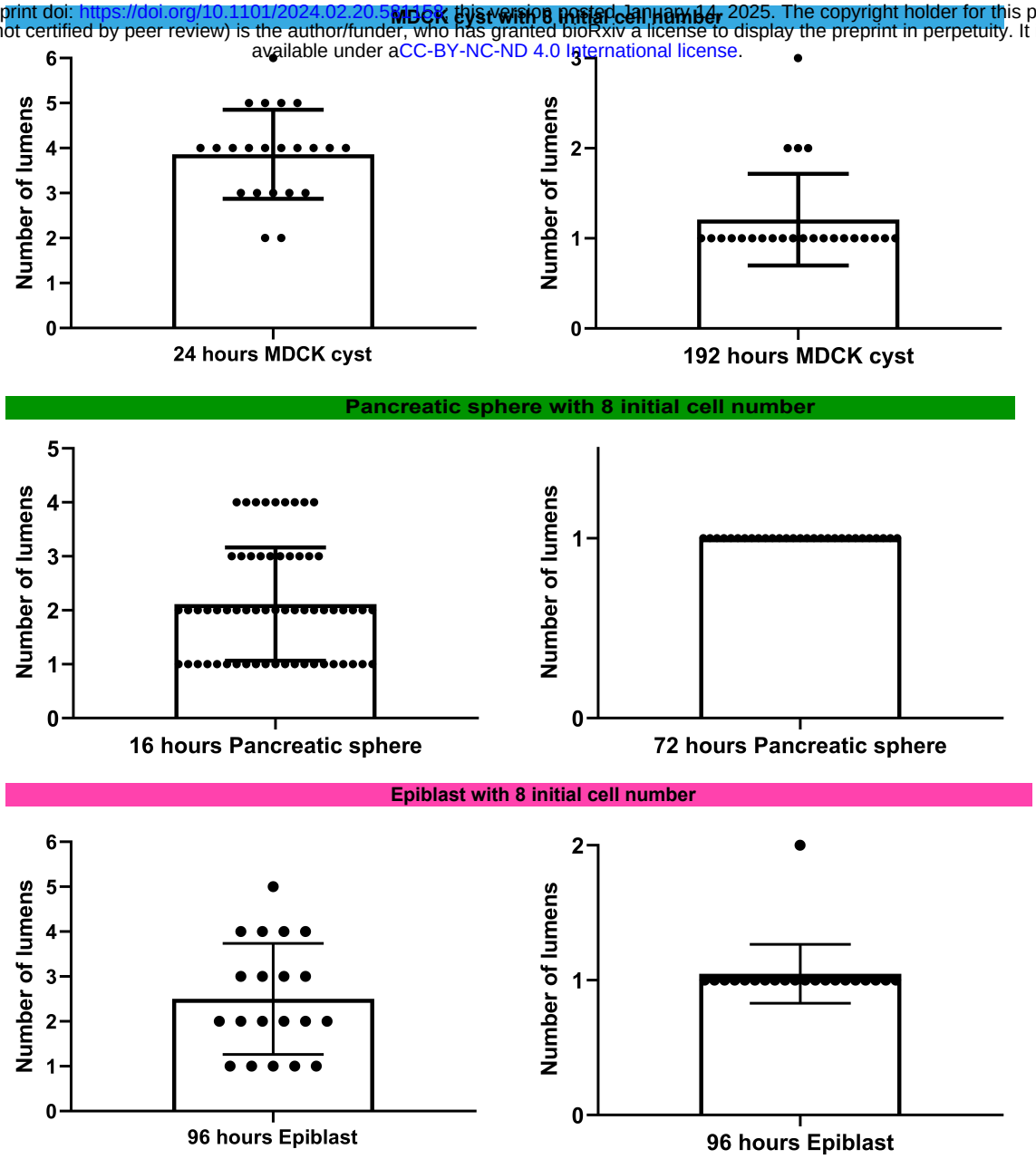

Extended Figure 3

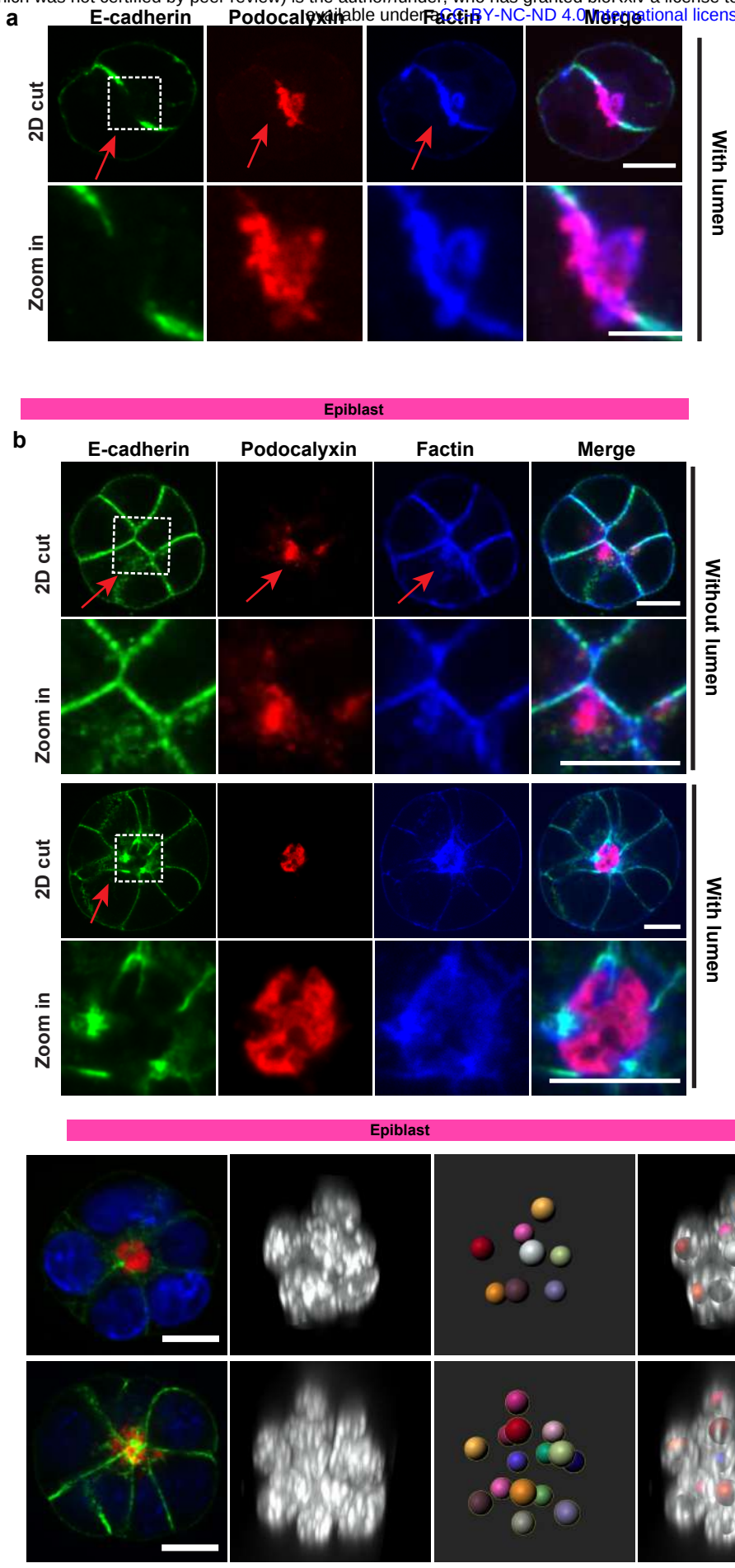

Extended Figure 4

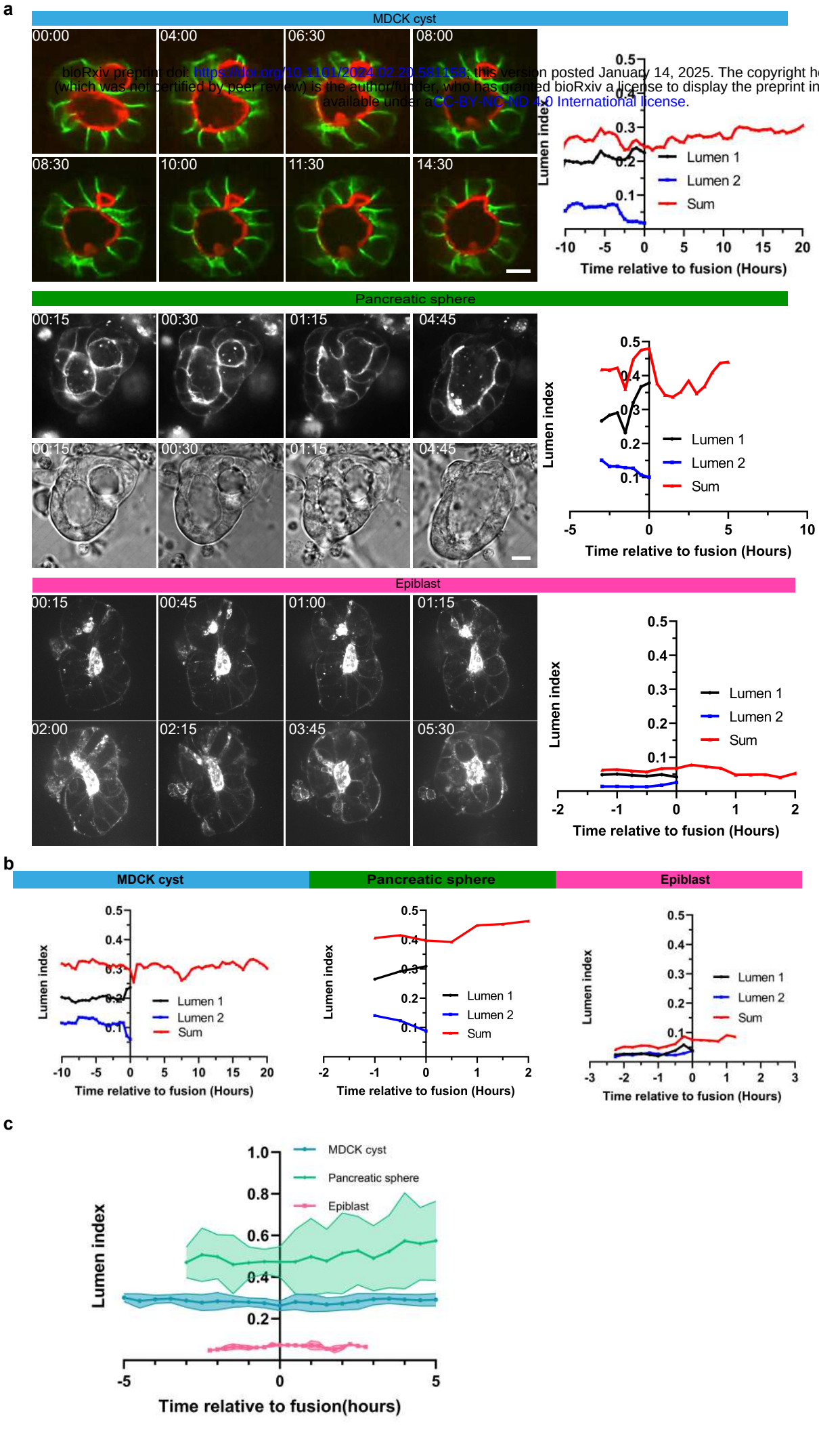

Extended Figure 5

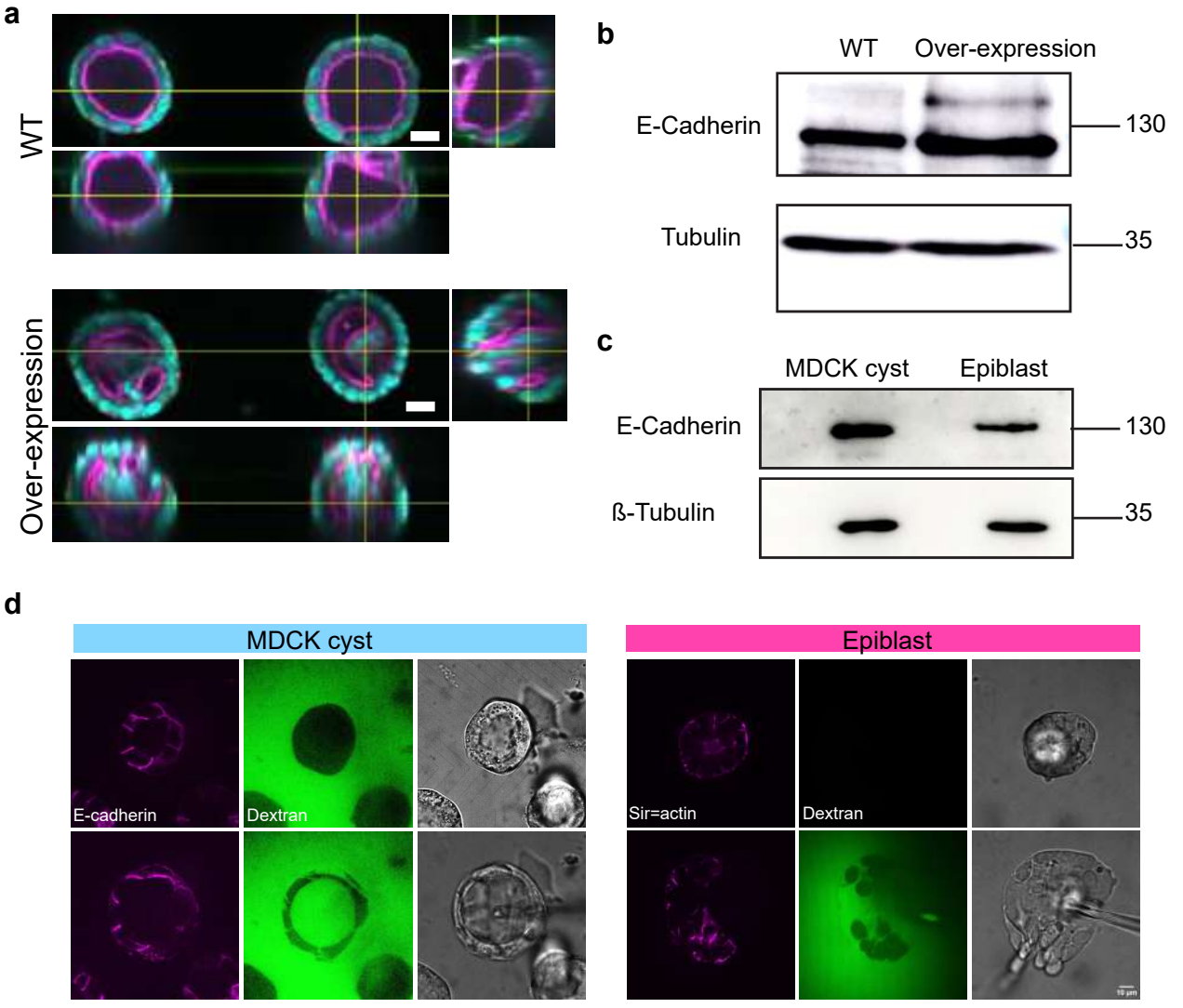

Extended Figure 6

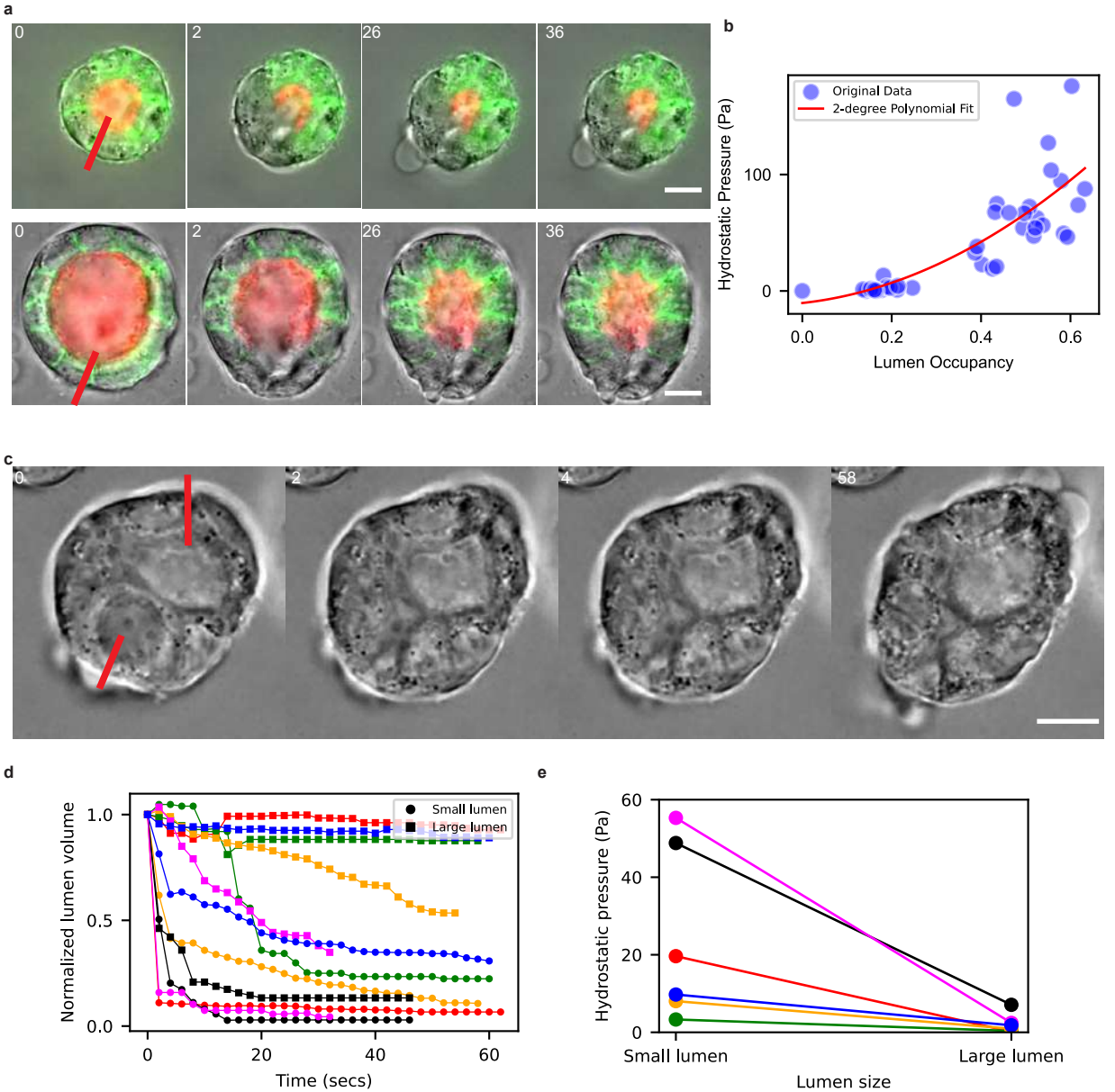

Extended Figure 7

a

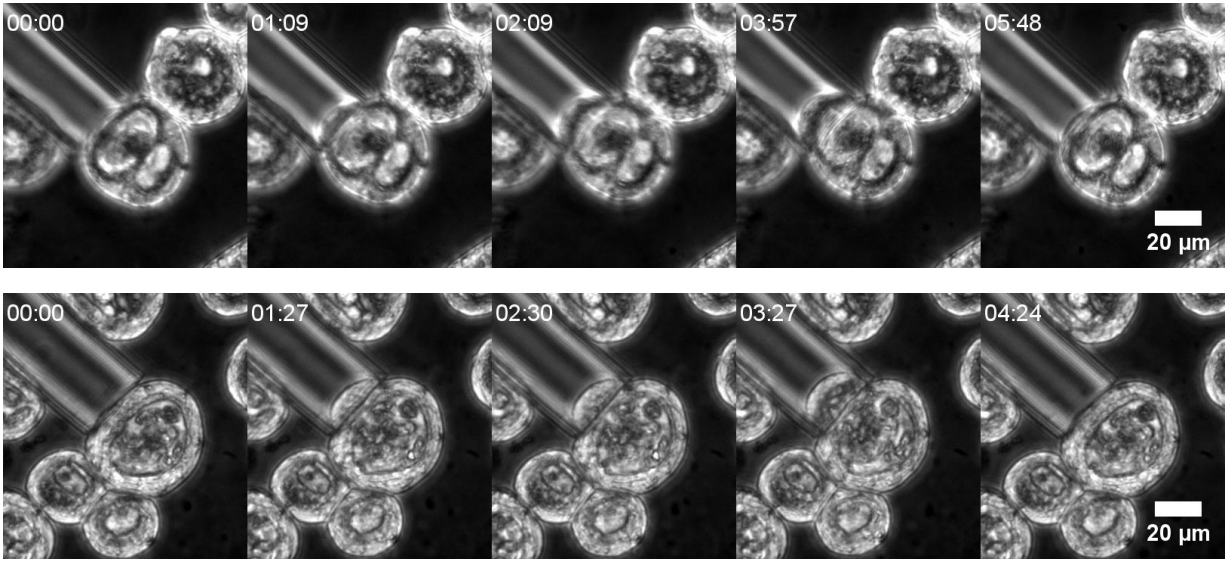

b

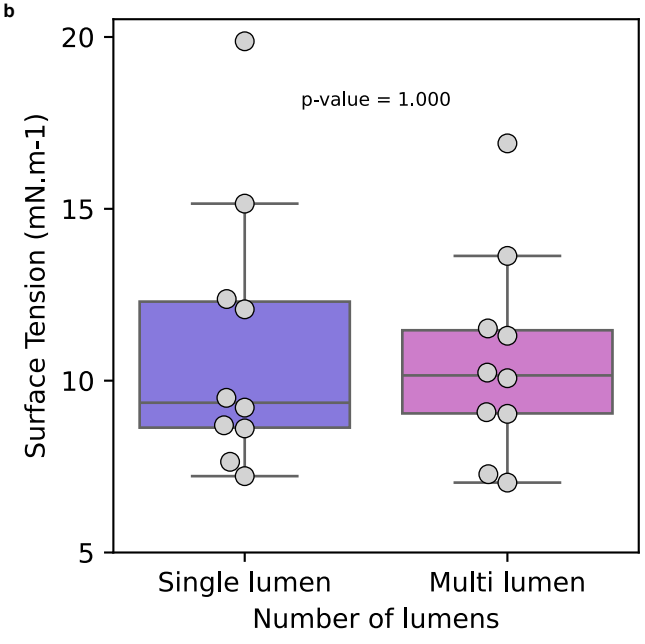

Extended Figure 8

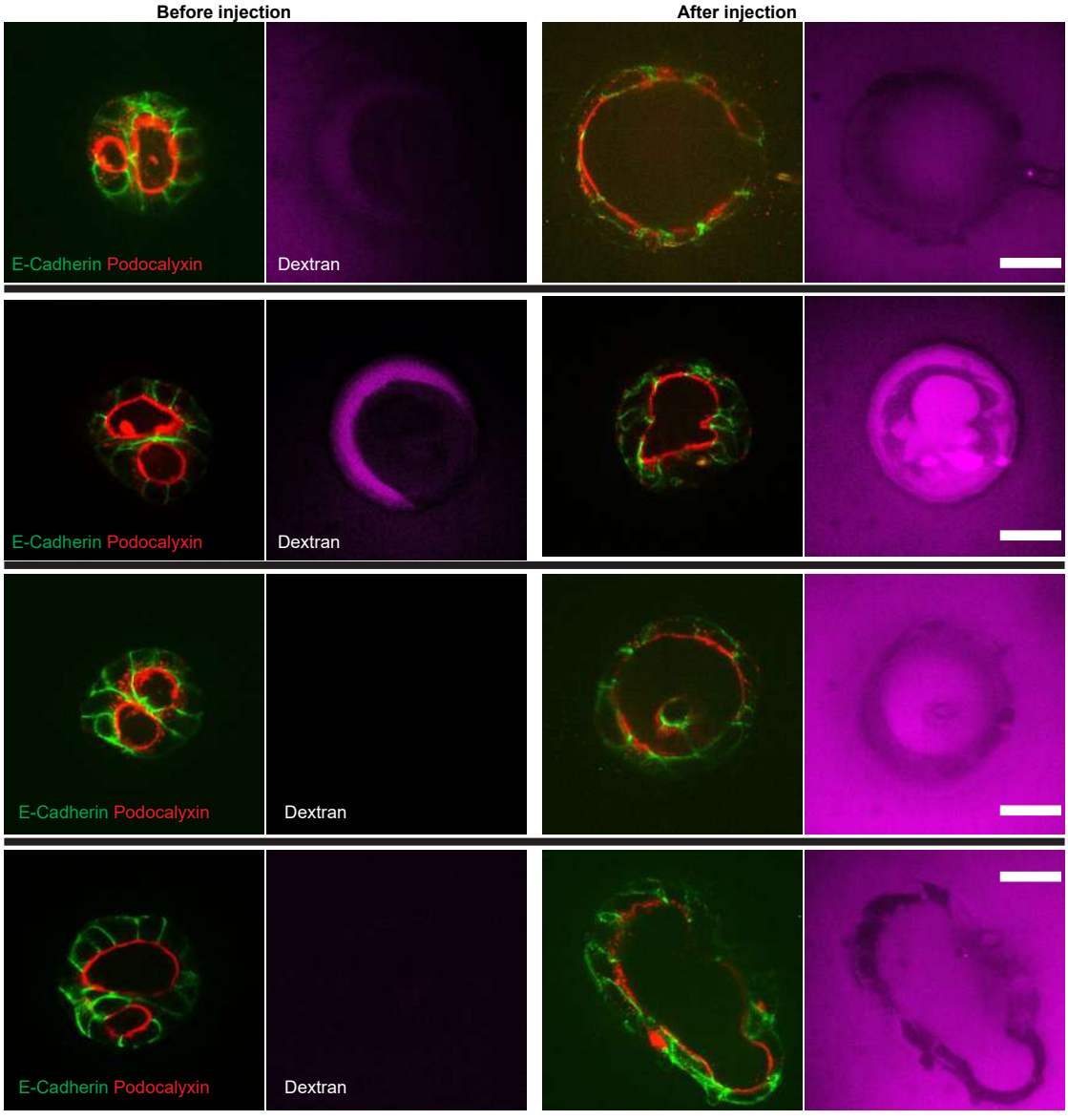

Extended Figure 9

a

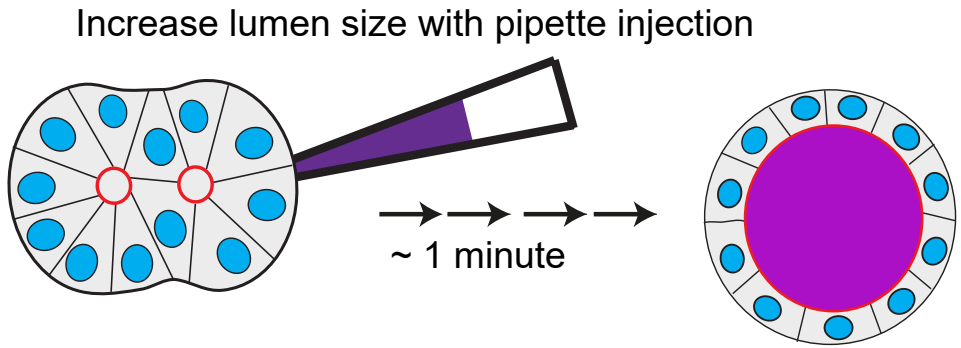

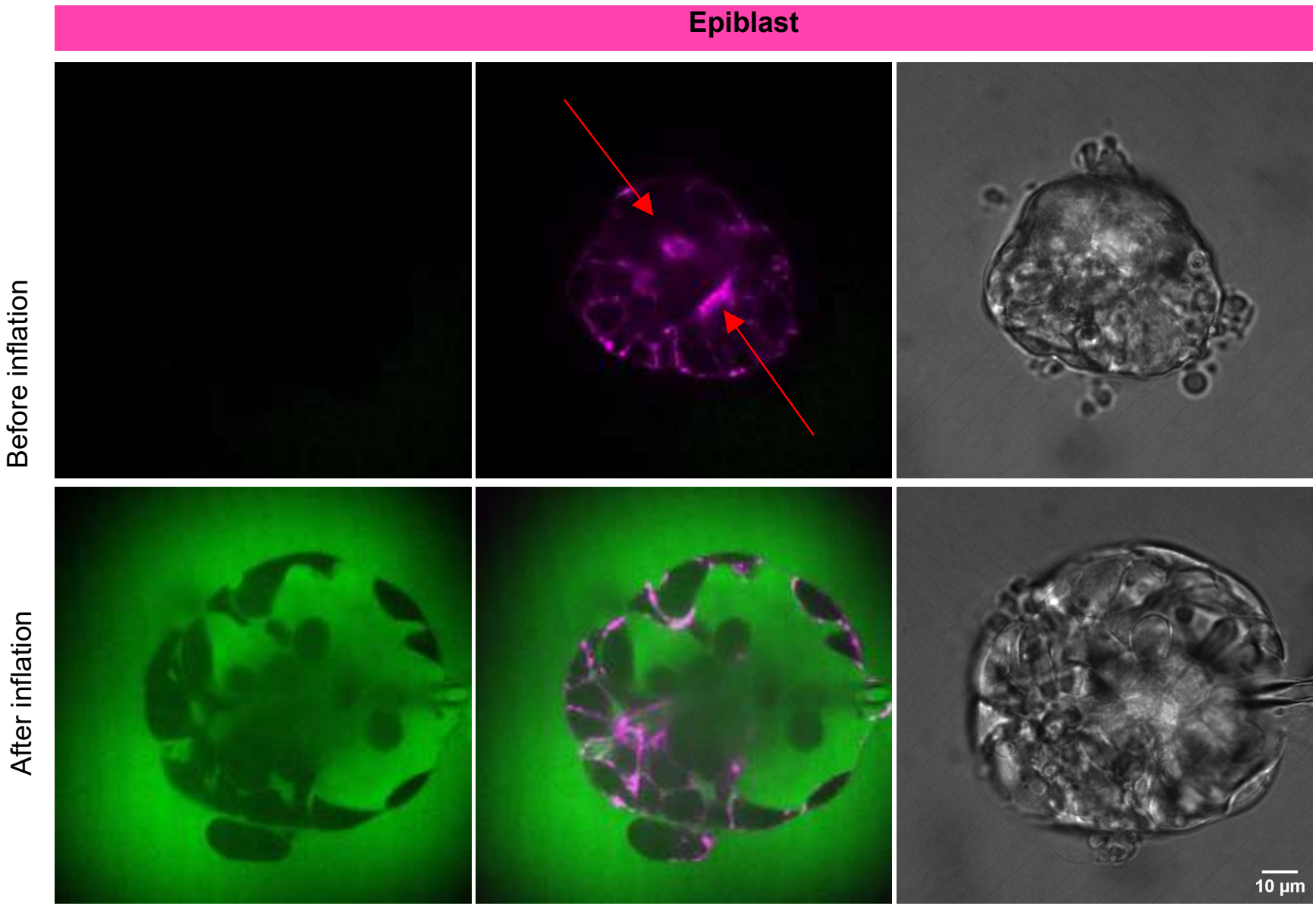

Extended Figure 10

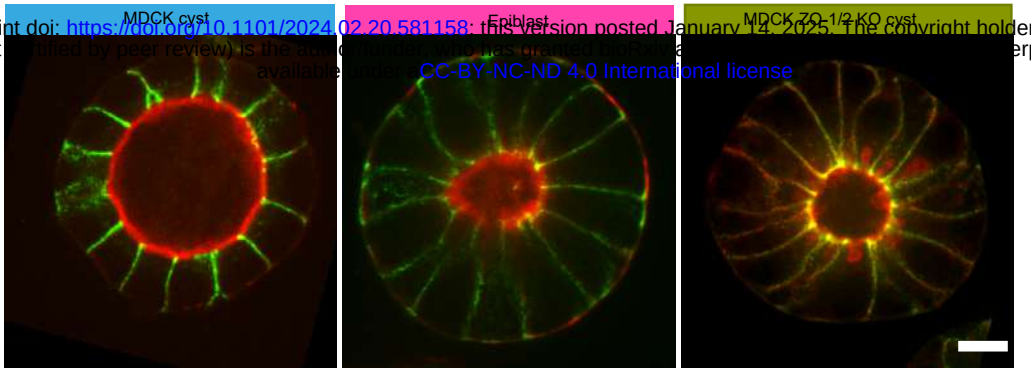

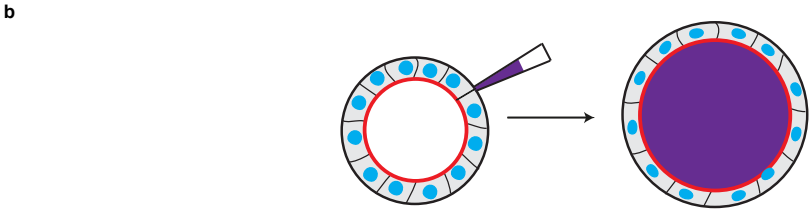

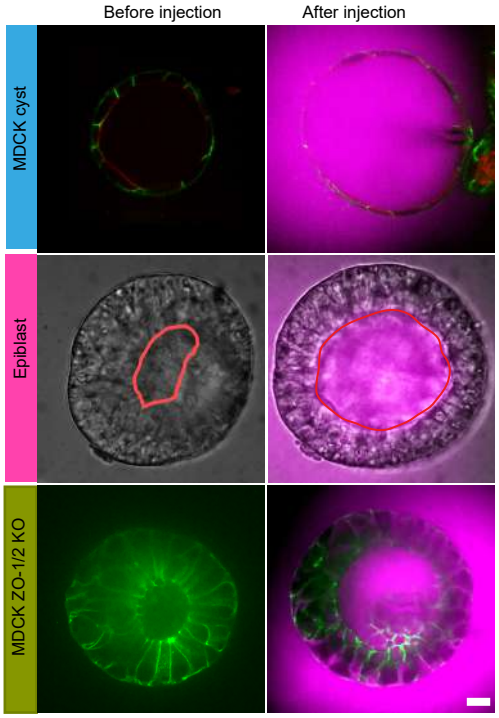

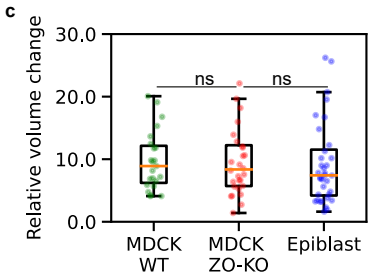

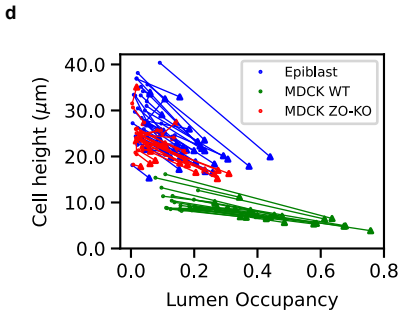

Extended Figure 11